# The question of laser wavelength for filling magnetic confinement machines with laser produced plasmas

L. L. Lengyel

IPP 4/131 July 1975

MAX-PLANCK-INSTITUT FÜR PLASMAPHYSIK

GARCHING BEI MÜNCHEN

**MAX-PLANCK-INSTITUT FÜR PLASMAPHYSIK**

**GARCHING BEI MÜNCHEN**

# The question of laser wavelength for filling magnetic confinement machines with laser produced plasmas

L. L. Lengyel

IPP 4/131 July 1975

*Die nachstehende Arbeit wurde im Rahmen des Vertrages zwischen dem Max-Planck-Institut für Plasmaphysik und der Europäischen Atomgemeinschaft über die Zusammenarbeit auf dem Gebiete der Plasmaphysik durchgeführt.*

IPP 4/131

# The question of laser wavelength for filling magnetic confinement machines with laser produced plasmas

L.L. Lengyel

July 1975


## Abstract

Radiation absorption and bulk ionization efficiencies are considered in a one-dimensional hydrodynamic approximation by taking finite rate ionization and recombination processes into account. The magnetic field effect on the plasma motion is taken into account by assuming that the plasma remains diamagnetic during its spherical expansion phase. At the moderate laser flux intensities and associated corona temperatures considered classical absorption is the dominating energy transfer mechanism, and the shorter the wavelength the better are the attainable absorption and ionization efficiencies. However, even at anomalous absorption rates manifested by complete energy damping at the critical density, pellet thermalization and bulk ionization are found to be more efficient at shorter wavelengths. Neglecting the finite ionization and recombination rates may lead to errors in predicting the location of the cutoff electron density layer and of the obtainable bulk ionization degree. The formation of a high-density high-temperature plasma sheath with appreciable polarization across the sheath is shown to take place at the plasma cloud magnetic field interface. Methods for avoiding the $\vec{v} \times \vec{B}$-induced drift motion associated with non-symmetric pellet irradiation are outlined.

## INTRODUCTION

The possibility of filling magnetic confinement machines with laser produced plasmas is attracting steadily increasing attention. The method, if it works, offers a number of advantages that are not matched by other filling methods:

1) The plasma can be produced directly at the magnetic axis, thus avoiding contact with material walls and reducing the level of impurities.

2) The size of the pellet to be ionized may be selected in such a way as to assure a specific initial plasma density in the volume to be filled.

3) The laser energy may be selected in such a way as to assure a particular initial temperature of the plasma produced.

4) The plasma thus obtained carries no net current and thus has minimum effect on the confining field.

A unique feature of laser produced plasmas is the possibility of selecting the temperature and density of the required plasma independently of each other for a wide range of temperature and density values. The limiting factor in selecting the plasma parameters seems to be the cost of the laser itself: by setting the desired plasma temperature or plasma density too high, the price of the laser required may be prohibitive, particularly for the large-scale magnetic confinement machines presently under construction.

The cost factors warrants careful consideration regarding the efficiency of the pellet heating and ionization processes and hence detailed analyses concerning the optimum laser parameters: energy, pulse-width, and wavelength.

Various institutes are, or have been, engaged in research, both theoretical and experimental, aiming at the fundamental characteristics of laser produced plasmas confined by magnetic fields. Some of the major activities are as follows:

The capture and confinement of laser produced plasmas in a minimum-B mirror field was extensively studied by A.F. Hought and associates at the United Aircraft Research Laboratories [1]. The ultimate goal of these investigations is the use of laser produced plasmas as target plasma for neutral beam injection. The same idea, i.e. laser produced plasma target for neutral beam injection is being pursued at LLL in Livermore, Calif. (the Baseball-II mirror experiment [2]).

One of the first experiments in Europe aimed at the magnetic confinement of laser produced plasmas was done by Tonon [3]. The same problem was also considered by Spalding and co-workers in Culham [4].

The capture and confinement of laser produced plasmas in a toroidal quadrupole magnetic field was studied by Friedman and Lubin at the University of Rochester [5]. In these experiments LiH pellets 100 $\mu$ in dia were shot at with a 3 J/20 ns ruby laser. Ten per cent of the pellet mass is reported to be trapped by the magnetic field ($n \approx 3 \times 10^{12}$ cm$^{-3}$, $Te \simeq 10$ eV).

The interaction of laser produced plasmas with magnetic fields (linear and cusp fields) is being studied extensively by T. Sekiguchi (University of Tokyo) and his group at the Institute of Plasma Physics, University of Nagoya [6]. The complementary theoretical investigations are carried out at the University of Tokyo. If the preliminary experiments prove to be successful, the method shall be applied for filling a large-scale spindle-cusp machine (an experiment with RF plugging along the line aperture) with laser produced plasmas.

The filling of Stellarators with laser produced plasmas has been studied at the University of Texas, Austin [7], and, rather extensively, at the Lebedev Institute of the Ac. Sci. U.S.S.R. in Moscow. According to Voronov [8], in the experiments at Lebedev Institute 10 % of the particles were captured by the Stellarator field (up to 30 % by a linear magnetic field). The confinement time recorded was in full agreement with the neoclassical diffusion theory. Another Stellarator vessel is supposed to be constructed at Lebedev Institute with special regard to laser plasma production (the number and location of port holes, their size, etc.).

Lastly, a new project group has been created at IPP Garching whose objective is to prove the feasibility of filling magnetic confinement machines with laser produced plasmas. The reliability of the method is to be tested in 1976 on the Wendelstein-IIB Stellarator, which is to be filled with a hydrogen or deuterium plasma produced by a 100 J/30 ns Nd-glass laser. The results of numerical calculations leading to the choice of this particular laser shall be summarized herein.

## STATEMENT OF THE PROBLEM

The fundamental problem in laser produced plasmas is the effectiveness of the beam plasma interaction, i.e. the efficiency of the energy transfer process from the laser beam to a highly inhomogeneous, partly cold and partly very hot (fully ionized) target material. The rate at which energy is deposited (absorbed) in a target plasma is a function of the local state parameters (of their gradients as well if anomalous processes are considered) and of the ratio of the laser beam frequency to the local plasma electron frequency. Hence for a given laser

wavelength the rate of energy absorption and the locus where energy is absorbed are functions of the plasma parameter distributions and thus of the dynamics of the plasma expansion itself.

Note that if filling of magnetic configurations with laser plasmas is considered, the absorption efficiency alone is not a criteria of effectiveness. The energy absorbed must be reasonably well distributed over the mass of the target material, otherwise the particle confinement characteristics may become very poor. If only a small number of particles are heated to very high temperatures, the magnetic field may not be sufficient to confine these particles and to prevent their loss to the walls. Besides, flares of high-energy particles may impair the stability of the whole confinement process. Furthermore, the part of the target material left behind as unionized gas is not confined by the magnetic field and may reach the wall, thus causing desorption (poor vacuum, impurities, etc.).

Opinion regarding the optimum laser wavelength for magnetic confinement plasmas seems to be divided. Some people advocate longer wavelengths ($CO_2$ laser, $\lambda = 10.6\ \mu$) because the corresponding cutoff density is lower ($10^{19}\ cm^{-3}$) and the expanding plasma may supposedly be heated through a longer fraction of the total expansion time. Furthermore, the threshold laser beam intensity characterising the onset of parametric decay instabilities decreases with increasing wavelength, and so it might be expected that the absorption efficiency enhanced by anomalous processes may be better, even at moderate flux intensities, if lasers with longer wavelengths are used. On the other hand, it is believed that shorter wavelengths (Nd-glass laser, $\lambda = 1.06\ \mu$, $n_{cutoff} = 10^{21}\ cm^{-3}$) heat the pellet core more efficiently because the energy is deposited at higher densities (closer to the cold core), and fewer extra-thermal runaway particles are produced in the high-temperature corona. Also the bulk temperature of

the expansion fan is supposed to be lower at shorter wavelength because of the larger mass present in the absorption zone.

Since at the time prior to the writing of this report no detailed calculations were available on the effect of the laser wavelength on the bulk efficiencies of the pellet heating and ionization processes as applied to magnetically confined plasmas, it has been decided to perform one-dimensional numerical calculations incorporating all relevant effects that - in combination with the laser wavelength - may influence the effectiveness of filling magnetic fields with laser produced plasmas.

In particular, it was hoped to clarify the following questions:

a) effect of the laser wavelength on the dynamics of the plasma heating and expansion, on the bulk absorption - and ionization efficiencies in particular;

b) effect of finite rate ionization and recombination processes on the bulk ionization efficiency;

c) effect of the pellet size and pellet-beam geometry (slab, cylindrical, and spherical symmetry) on the plasma expansion and absorption characteristics;

d) an estimate of the magnetic field effects (in one-dimensional approximation) on the above processes.

A Lagrangean code capable of handling, one-dimensional cases with slab, cylindrical, and spherical symmetry, and incorporating the following main features has been developed:

a) either classical (collisional) absorption, or 100 % energy damping at the critical density region;

b) collisional ionization, photo-ionization and recombination processes;

c) temperature-dependent ("nonlinear") thermal conductivity;

d) diamagnetic flow-work, as a result of expansion in a magnetic field.

Anomalous absorption - which is rather difficult to incorporate in a hydrodynamic code - was modelled simply by 100 % energy damping at the critical density (an alternative to classical absorption).

## I. MATHEMATICAL MODEL

### I/1 Conservation equations

The set of conservation equations used in the present approximation is as follows:

$$\frac{\partial m_e}{\partial t} + \nabla\cdot(\vec{u} m_e) = \dot{m}_e = \dot{I} - \dot{R} \quad , \tag{1.1}$$

$$\frac{\partial m}{\partial t} + \nabla\cdot(\vec{u} m) = 0 \quad , \tag{1.2}$$

$$\rho\left(\frac{\partial}{\partial t} + \vec{u}\nabla\right)\vec{u} = -\nabla(p+q) \quad , \tag{1.3}$$

$$\frac{d}{dt}\left(\frac{3}{2} m k T\right) + \frac{5}{2} m k T \nabla\cdot\vec{u} = -\nabla\cdot\vec{\phi} + \nabla\cdot(\varkappa \nabla T) - \epsilon_i \dot{n}_e \quad , \tag{1.4}$$

$$\text{where} \quad p = m k T \quad \text{and} \quad T = e / c_v \quad . \tag{1.5}$$

In the above equations, besides the commonly used symbols the following notation has been introduced: $q$ - artificial viscosity, e - specific internal energy, $\varkappa$ - electron thermal conductivity, $\vec{\phi}$ - laser beam intensity, $\epsilon_i$ - ionization potential, $\dot{I}$ and $\dot{R}$ - ionization and recombination rates, respectively, and $\dot{n}_e = \dot{I} - \dot{R}$. The equation of state of an ideal gas has been assumed to be applicable.

Owing to the high collision frequency inherent in the first phase of the plasma expansion the electron-ion equilibration time is negligible and the use of a single-temperature model appears to be reasonable.

## I/2. Radiation absorption

Collisional absorption (inverse bremsstrahlung) is assumed to be the only mechanism responsible for energy deposition. Thus, the spatial variation of the laser flux intensity in the direction of the laser beam is given by

$$\phi(s,t) = \phi_L(t)\exp\left(-\int \bar{K}_{ei}\,ds\right) \tag{1.6}$$

where $\phi_L$ is the impinging laser flux intensity and $K_{ei}$ is the absorption coefficient [9]:

$$\bar{K}_{ei}\left(\frac{1}{cm}\right) = 1.21\times10^{-10}\frac{\ln\Lambda\, n_e^2}{n_{e\,crit}\left(k\bar{T}_e\right)^{3/2}}\left(1-n_e/n_{e\,crit}\right)^{-1/2} \tag{1.7}$$

$ne_{crit}$ being the critical (cutoff) electron density corresponding to $\omega_l = \omega_{pe}$ (laser frequency = plasma electron frequency). $n_e$ and kTe are given in ($cm^{-3}$) and (keV), respectively.

## I/3. Thermal conductivity

Spitzer's thermal conductivity [10] (Lorentz gas approximation, fully ionized plasma) has been used for the electron component:

$$\lambda_e = 20\left(\frac{1}{\pi}\right)^{3/2}\frac{\left(k\bar{T}_e\right)^{5/2}}{m_e^{1/2}\,e^4\,Z\,\ln\Lambda} \approx \frac{5.85\times10^{12}}{Z\cdot\ln\Lambda}\left[T_e(keV)\right]^{5/2} \tag{1.8}$$

ergs $\cdot$ (cm $\cdot$ sec $\cdot$ °K)$^{-1}$

Note that the effect of this nonlinear (temperature-dependent) thermal conductivity becomes noticeable only at temperatures above ~ 10 eV. Since at low temperatures thermal conduction does not play any practical role in

the energy transport (at the time scales considered), the accuracy of the calculations is not affected by using the same expression for relatively cold ($T_e < 10$ eV) partially ionized plasma regions.

## I/4. Ionization and recombination rates

In the analyses available on the dynamics of laser-produced plasmas it is usually assumed that the target material is ionized by multi-photon absorption and cascade ionization processes [1]. Analyses based on this model assume instantaneous ionization at the target surface and treat the plasma thus produced as a fully ionized substance during the expansion phase. Such an approximation is justified in investigations pertaining to inertial confinement and laser-induced fusion phenomena where the energy supply rates and the associated time scales are such that finite-rate relaxation processes may be omitted from consideration. However, when filling magnetic confinement machines with laser-produced plasmas is considered, finite rate relaxation processes may play a significant role in the resulting bulk absorption and ionization efficiencies. At the laser flux intensities considered the shock wave produced always precedes the thermal wave and the cold target material may become partially ionized by shock waves (particularly by reflected shocks) before getting exposed to laser radiation. Since light penetration stops at the critical density layer, parts of the matter heated may never get exposed directly to the laser light. Furthermore, for times associated with plasma production in magnetic confinement configurations recombination may appreciably change the electron density and the bulk ionization degree both during and after the laser pulse. Probe measurements performed by Friedman [5] could detect only a small fraction of the charged particles predicted by computer calculations without taking finite rate ionization and recombination processes into account.

Interferometric measurements of Büchl and Haering [12] yielded charged particle numbers notably less than those predicted by the similarity models available.

It has thus been decided to perform numerical calculations with finite ionization and recombination rates.

Collisional ionization, photo-ionization and recombination processes have been taken into account in determining the electron/ion production rates. Hence

$$\dot{n}_e = Z\dot{n}_i = n_e n_n \alpha_c - n_e^2 n_i \beta_c + n_n \alpha_\gamma - n_e n_i \beta_\gamma \qquad (1.9)$$

where $\alpha_c$, $\beta_c$ represent collisional ionization and recombination rates,

$\alpha_\gamma$, $\beta_\gamma$ are the photo-ionization and recombination rates, respectively.

Since $n_e = Z n_i$ and using the condition of detailed equilibrium, where the equilibrium electron density is assumed to be given by the Saha value (denoted hereafter by $n_{es}$) we have

$$n_{es} n_n \alpha_c = n_{es}^3 \beta_c / Z \;; \rightarrow \quad \alpha_c = n_{es}^2 \beta_c / n_n Z$$

$$n_n \alpha_\gamma = n_{es}^2 \beta_\gamma / Z \;; \rightarrow \quad \alpha_\gamma = n_{es}^2 \beta_\gamma / n_n Z$$

and thus for hydrogen-like atoms (Z = 1)

$$\dot{n}_e = (n_{es}^2 - n_e^2)(n_e \beta_c + \beta_\gamma) \qquad (1.10)$$

The recombination rate coefficients and are unique functions of the electron temperature [12]:

$$\beta_c = 8.75 \times 10^{-27} / [\,T_e(eV)\,]^{9/2} \quad cm^6/sec$$

$$\beta_\gamma = 2.70 \times 10^{-13} / [\,T_e(eV)\,]^{3/4} \quad cm^6/sec \qquad (1.11)$$

The ratio

$$\beta_{\ni}/n_e\beta_c \approx 0.31\times10^{14}\,[T_e(eV)]^4 / [n_e(cm^{-3})]$$

represents the weighting factor for radiative processes. As can be seen, at sufficiently high temperature photo-ionization and radiative recombination may be dominant for a wide range of electron density values (the expansion fan of laser produced plasmas).

In view of eqs. (1.2) and (1.9) eq. (1.1) can be rewritten in the following form:

$$\frac{d}{dt}(\ln n_e) = (n_{es}^2 - n_e^2)(\beta_c + \beta_{\ni}/n_e) + \frac{d}{dt}(\ln\varrho) \qquad (1.12)$$

Since the relative change of the electron density is usually greater than the relative density change (ionization takes place in a medium that itself is being compressed), the term $d\ln\varrho/dt$ on the r.h.s. of eq. (1.12) may be neglected in the first approximation and the solution thus obtained may be corrected subsequently for the volumetric dilution characterizing the perticular time increment (a two-step iterative procedure). Furthermore, if one evaluates the recombination rate coefficients $\beta_c$ and $\beta_{\ni}$ at an effective (mean) temperature characterizing a certain time interval (time increment), the integral of the equation

$$\frac{dn_e}{dt} \approx (n_{es}^2 - n_e^2)(\beta_c n_e + \beta_{\ni})$$

may be obtained analytically:

$$\beta_c \ln\frac{\beta_{\ni} + n_a\beta_c}{\beta_{\ni} + n_a\beta_e} - \frac{1}{2}\beta_c \ln\frac{n_{es}^2 - n_e^2}{n_{es}^2 - n_a^2} -$$

$$-\frac{\beta_{\ni}}{2n_{es}}\ln\left(\frac{n_{es}+n_e}{n_{es}-n_e}\cdot\frac{n_{es}-n_a}{n_{es}+n_a}\right) = \left[(\beta_c n_{es})^2 - \beta_{\ni}^2\right]\Delta t \qquad (1.13)$$

where $n_a = n_a(t)$ and $n_e = n_e(t+\Delta t)$ represent the initial and final electron densities, respectively, and

$n_{e,s} = n_{e,s}(t+\Delta t)$ is the equilibrium (Saha) electron density corresponding to the effective (mean) electron temperature characterizing the particular time interval $\Delta t$ :

$$n_{e,s} = \alpha n_n \text{ , where } \alpha = \tfrac{1}{2} f_1 \left[ \left( 1 + 4./f_1 \right)^{1/2} - 1 \right] \text{, and}$$

$$f_1 = 2 (g_1/g_0) \frac{1}{n_n} \left( 2\pi m_e k T_e / h^2 \right)^{3/2} \exp\left( - \epsilon_i / k T_e \right)$$

represents the Saha function. In the case of hydrogen, the partition function ratio is given as $g_1/g_0 = 1/2$ .

Unfortunately, eq. (1.13) cannot be solved explicitly for $n_e$ . However, explicit expressions can be obtained for the two limiting cases where either collisional processes or photo-processes dominate.

a) If collisional processes dominate over the respective radiative ones $\beta_\gamma / n_e \beta_c \ll 1$ and eq. (1.13) reduces to

$$\left( n_e / n_{e,s} \right)_{coll} = \left[ \frac{\exp(\Delta t/\tau_c)}{\exp(\Delta t/\tau_c) + (n_{e,s}/n_a)^2 - 1} \right]^{1/2} \qquad (1.14)$$

where $\tau_c \equiv \left[ 2 \langle \beta_c \rangle n_{e,s}^2 \right]^{-1}$ (1.15) represents the characteristic time for collisional recombination [13] corresponding to a recombination rate coefficient evaluated at the effective (mean) electron temperature: $\langle \beta_c \rangle = \beta_c(\langle T_e \rangle)$. As can be seen,

if $\Delta t / \tau_c \ll 1$

$n_e(t+\Delta t) \to n_a = n_e(t)$ (no relaxation at all);

if $\Delta t / \tau_c \gg 1$

$n_e(t+\Delta t) \to n_{e,s}(t+\Delta t)$ (complete relaxation).

b) If radiative processes dominate $\beta_\gamma / n_e \beta_c \gg 1$ and eq. (1.13) reduces to

$$\left( n_e / n_{e,s} \right)_{rad} = \frac{\exp(\Delta t/\tau_\gamma) - (n_{e,s} - n_a)/(n_{e,s} + n_a)}{\exp(\Delta t/\tau_\gamma) + (n_{e,s} - n_a)/(n_{e,s} + n_a)} \qquad (1.16)$$

where $\tau_\gamma \equiv [\, 2 \langle \beta_\gamma \rangle n_{e\zeta} \,]^{-1}$ (1.17)

represents the characteristic relaxation time for radiative processes. As before,

if $\Delta t / \tau_\gamma \ll 1$, $n_e(t+\Delta t) \to n_e(t)$ ;

if $\Delta t / \tau_\gamma \gg 1$, $n_e(t+\Delta t) \to n_{e\zeta}(t+\Delta t)$.

c) To construct a solution for the intermediate region $\beta_\gamma / n_e \beta_c \approx O(1)$, a linear combination of the solutions (1.14) and (1.16) with $\eta_\gamma \equiv \beta_\gamma / n_e \beta_c$ as a weighting factor has been used. Thus

$$\frac{n_e}{n_{e\zeta}} = \frac{1}{1+\eta_\gamma} \left[ \left( n_e / n_{e\zeta} \right)_{coll} + \eta_\gamma \left( n_e / n_{e\zeta} \right)_{rad} \right] \qquad (1.18)$$

## I/5. Magnetic field effects on plasma expansion

An accurate account of the interaction between a magnetic field and the expanding plasma cloud would require computing the instantaneous electromagnetic and current distributions in the plasma, i.e. the simultaneous solution of Maxwell's equations with those given in Sect. I/1. Besides, considering even the relatively simple case of spherical (more correctly: initially spherical) plasma expansion in a uniform magnetic field, the problem can no longer be treated in the framework of a one-dimensional (spherically symmetric) approximation because of the difference in the expansion dynamics along and across the magnetic field lines. A two-dimensional axially symmetric model would be the appropriate approach in this case. In the framework of the present approximation, we shall limit our considerations to estimating the maximum radius the plasma blob may reach while expanding across the magnetic field lines. It is assumed that the plasma corona surrounding the high-density core is fully ionized and the plasma volume remains diamagnetic during the first phase of the plasma expansion.

Consider a volume V filled initially with a uniform magnetic field of strength $B_o$. The work necessary for making this volume diamagnetic by performing work against the magnetic pressure $B_o^2/2\mu_o$ is equal to $(B_o^2/2\mu_o)V$ . One can thus estimate the maximum possible plasma radius in a magnetic field by assuming that all energy absorbed is spent on flow-work against the magnetic pressure (zero kinetic and internal energies):

$$\frac{4}{3}\pi R_{max}^3 \frac{B_o^2}{2\mu_o} = Q_{absorb.}$$

and thus

$$R_{max} = \left(\frac{1.5\mu_o}{\pi}\right)^{1/3} Q_{absorb}^{1/3} B_o^{-2/3} \qquad (1.19)$$

Of course, the actual radial plasma dimension is always less than the value given by eq. (1.19) because the plasma gains considerable momentum along the magnetic field lines long before the motion ceases in the radial direction. Furthermore, there will always be kinetic and internal energies present in the expanding plasma, which again reduced the maximum obtainable radial dimension.

In actual numerical calculations it has been assumed that the plasma cloud behaves like an ideally conducting sphere, stretching the magnetic field lines while expanding in the magnetic field. The distribution of the magnetic flux lines around an ideally conducting sphere placed in a uniform magnetic field - just as its classical hydrodynamic analogue (streamline distribution over a spherical obstacle placed in an inviscid uniform flow) - is well known [14, 15].

The corresponding potential function (see Fig. 1) is

Fig. 1

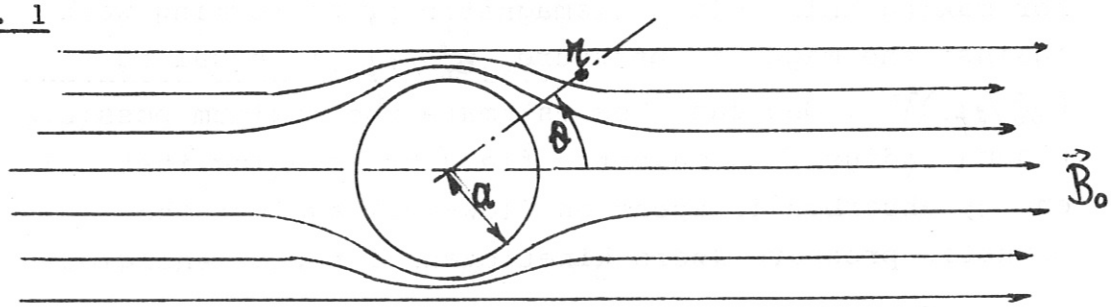


$$\phi = \tfrac{1}{2} B_0 \left( 2r + a^3/r^2 \right) \cos\theta \,, \qquad (1.20)$$

and thus

$$B_r = B_0 \left[ 1 - \left( a/r \right)^3 \right] \cos\theta$$

$$B_\theta = B_0 \left[ 1 + \tfrac{1}{2} (a/r)^3 \right] \sin\theta$$

and

$$p_{magn} = B^2/2\mu_0 = \frac{1}{2\mu_0} \left( B_r^2 + B_\theta^2 \right) \qquad (1.21)$$

The maximum value of the magnetic pressure at the surface of the sphere is equal to $9B_0^2/8\mu_0$ . In the numerical calculations, one may use either this value or the mean pressure over the surface or just the unperturbed magnetic pressure value ( $B_0^2/2\mu_0$ ) as boundary condition for the expanding plasma cloud.

## II. WORKING EQUATIONS

Noting that $\varrho = n m_a$ , $T = e/c_v$ , where $\varrho$ and $e$ denote mass density and specific internal energy, respectively, the one-dimensional variant of eqs. (1.1) to (1.5) may be rewritten in the following form:

$$\frac{\partial \varrho}{\partial t} + \frac{1}{r^a} \frac{\partial}{\partial r} \left( r^a \varrho u \right) = 0 \,, \qquad (2.1)$$

$$\frac{du}{dt} + \frac{1}{\varrho} \frac{\partial}{\partial r} \left( p + q \right) = 0 \,, \qquad (2.2)$$

$$\frac{de}{dt} + \left( p + q \right) \frac{dV}{dt} = \frac{1}{r^a \varrho} \frac{\partial}{\partial r} \left( -r^a \phi + r^a \frac{\lambda}{c_v} \frac{\partial e}{\partial r} \right) - \epsilon_i \frac{\dot{n}_e}{\varrho} \,, \qquad (2.3)$$

$$p = (\gamma-1)\rho e .$$

Here $r$ denotes distance measured from the center of the coordinate system and $a$ = 0, 1, 2 correspond to slab, cylindrical, and spherical symmetry, respectively.

The total energy equation (used for integral checks) is obtained by adding the product of eq. (2.2) and the velocity to eq. (2.3):

$$\rho \frac{d}{dt}\left( e + \tfrac{1}{2}u^2 \right) + \frac{1}{r^a}\frac{\partial}{\partial r}\left[ r^a u (p+q) \right] =$$

$$= \frac{1}{r^a}\frac{\partial}{\partial r}\left( -r^a \phi + r^a \frac{\partial e}{c_v}\frac{\partial e}{\partial r} \right) - \epsilon_i \dot{m}_e \qquad (2.4)$$

On the basis of eq. (2.1) a stream function may be defined such that

$$r^a \rho = \frac{\partial \psi}{\partial r} , \qquad r^a \rho u = -\frac{\partial \psi}{\partial t} , \qquad (2.5)$$

$$\text{i.e.} \qquad \rho = (1/r^a)\,\partial\psi/\partial r , \qquad (2.5a)$$

which may then be used as a Lagrangean mass coordinate. Note that $d\psi = r^a \rho (dr - u dt)$, which at any given time instant (dt = o) represents the mass contained in a gas layer of thickness $dr$ (mass/rad and mass/sterad in the case of cylindrical and spherical geometries, respectively).

The transformation formulae from the old (Eulerian) to the new (Lagrangean) coordinates are

$$\frac{\partial}{\partial r} = r^a \rho \frac{\partial}{\partial \psi} ,$$

$$\frac{\partial}{\partial t} = -r^a \rho u \frac{\partial}{\partial \psi} + \frac{\partial}{\partial t} , \qquad (2.6)$$

$$\frac{d}{dt} \equiv \frac{\partial}{\partial t} + u\frac{\partial}{\partial r} = -r^a \rho u \frac{\partial}{\partial \psi} + \frac{\partial}{\partial t} + u r^a \rho \frac{\partial}{\partial \psi} = \frac{\partial}{\partial t} .$$

The set of equations (2.1) to (2.4) supplemented by eq. (2.5a) can thus be written as follows:

$$\frac{\partial u}{\partial t} = -r^a \frac{\partial}{\partial \psi}(p+q)\,, \tag{2.7}$$

$$\frac{\partial r}{\partial t} = u\,, \tag{2.8}$$

$$V = r^a \frac{\partial r}{\partial \psi}\,, \quad \rho = V^{-1} \tag{2.9}$$

$$\frac{\partial e}{\partial t} = -p\frac{\partial V}{\partial t} - q\frac{\partial}{\partial \psi}(r^a u) + \frac{\partial}{\partial \psi}(-r^a \phi) + \\ + \frac{\partial}{\partial \psi}\left(r^{2a}\rho \frac{\varkappa}{c_v}\frac{\partial e}{\partial \psi}\right) - \epsilon_i \frac{\dot{n}_e}{\rho}\,, \tag{2.10}$$

$$\rho \frac{\partial}{\partial t}(e+\tfrac{1}{2}u^2) = -\rho\frac{\partial}{\partial \psi}\left[r^a u(p+q)\right] + \\ + \rho\frac{\partial}{\partial \psi}\left[-r^a\phi + \rho r^{2a}\frac{\varkappa}{c_v}\frac{\partial e}{\partial \psi}\right] - \epsilon_i \dot{n}_e \tag{2.11}$$

where, as before, $p = (\gamma-1)\rho e$ , and the artificial viscosity $q$ is given as

$$q = -\,\text{Const}\,\rho\left(\frac{\partial u}{\partial \psi}\right)^2_{min}\,; \quad \left.\frac{\partial u}{\partial \psi}\right)_{min} = \min\left(0, \frac{\partial u}{\partial \psi}\right) \tag{2.12}$$

i.e. it is either positive or zero.

## II/1. Reduced coordinates

As reference quantities the state parameters $T_o$ , $\rho_o$ and the characteristic dimension $l_o$ of a deuterium ice pellet shall be used. Ideal gas relations are assumed to be valid. The magnetic field strength is given as $B_o$.

The numerical values used in this set of calculations are as follows:

$T_o = 18.7\,^\circ K$ (triple point temperature, deuterium ice),

$\rho_o = 0.196\ gr/cm^3$ (deuterium ice density)

$l_o = 500\ \mu$ (typical pellet dimension), and

$B_o$ = 1 tesla.

The rest of the reference values can thus be computed as follows ( $m_D = 3.346 \times 10^{-27}$ kgm , $k/m_D = 4.12 \times 10^3$ J/kgm°K , $c_v = 3k/2m_D = 6.19 \times 10^3$ J/kgm°K , $\epsilon_i = 13.6$ eV + + 2.24 eV dissoc. energy = 15.84 eV ) :

$$n_o = m_D^{-1} \rho_o \,, \qquad m_o = \rho_o l_o^3$$

$$e_o = c_v T_o \,, \qquad \psi_o = \rho_o l_o^{a+1}$$

$$p_o = mkT_o = (\gamma-1) e_o \rho_o \,, \qquad \phi_o = e_o \rho_o c_o$$

$$c_o = (\gamma p_o/\rho_o)^{1/2} \,, \qquad Q_o = e_o \rho_o l_o^3$$

$$\tau_o = l_o / c_o \,, \qquad q_o = \gamma^{-1} \rho_o^3 l_o^{2(a+1)} c_o^2 \psi_o^{-1} = p_o$$

$$p_{magn_o} = B_o^2 / 2\mu_o \,,$$

Reducing equations (2.7) to (2.12) by means of the reference values given here we obtain the following set of dimensionless equations:

$$\frac{\partial u}{\partial t} = -\frac{r^a}{\gamma} \frac{\partial}{\partial \psi}(p+q) \,, \tag{2.13}$$

$$\frac{\partial r}{\partial t} = u \,, \tag{2.14}$$

$$V = r^a \frac{\partial r}{\partial \psi} \,, \tag{2.15}$$

$$\frac{\partial e}{\partial t} = -(\gamma-1) p \frac{\partial V}{\partial t} - (\gamma-1) q \frac{\partial}{\partial \psi}(r^a u) + \frac{\partial}{\partial \psi}(-r^a \phi) + + \varepsilon_{diff} \frac{\partial}{\partial \psi}\left(r^{2a} \rho e^{5/2} \frac{\partial e}{\partial \psi}\right) - \varepsilon_{psion} \dot{n}_e / \rho \,, \tag{2.16}$$

$$\frac{\partial}{\partial t}\left[e + \tfrac{1}{2}\gamma(\gamma-1)u^2\right] + (\gamma-1)\rho \frac{\partial}{\partial \psi}\left[r^a u (p+q)\right] = = \frac{\partial}{\partial \psi}\left(-r^a \phi + \varepsilon_{diff} \rho r^{2a} e^{5/2} \frac{\partial e}{\partial \psi}\right) - \varepsilon_{psion} \dot{n}_e \,, \tag{2.17}$$

$$p = e\rho \,,$$

where the two dimensionless parameters $\mathcal{E}_{diff}$ and $\mathcal{E}'_{psim}$ appearing in the energy equations are defined as

$$\mathcal{E}_{diff} = \frac{\varkappa_0 / c_v}{\rho_0 c_0 l_0} \tag{2.18}$$

$$\mathcal{E}_{psim} = \frac{\epsilon_i n_0}{\rho_0 l_0} = \frac{\epsilon_i}{e_0 m_D} \tag{2.19}$$

(Subscript "o" after quantities such as $\varkappa$ denotes values evaluated under reference conditions $T = T_0$, $n = n_0$, etc.).

The absorption equation (1.6) is rewritten in dimensionless form:

$$\left.\begin{aligned} \phi(r,t) &= \phi_L(t) \exp\left(-C_{absrb} \int K_{ei}\, dr\right) \\ \text{where} \quad \phi_L(t) &= \left(\frac{Q_L(t)}{\tau_{pulse} \cdot a_{beam}}\right) \Big/ \left(e_0 \rho_0 c_0\right) \\ K_{ei} &= n_e^2 e^{-3/2} \left(1 - n_e / n_{ecrit}\right)^{-1/2} \end{aligned}\right\} \tag{2.20}$$

and

$$C_{absrb} = \frac{3.36 \ln\Lambda}{3 \times 10^{10}} \cdot \frac{l_0 n_0^2}{n_{crit} \cdot T_0^{3/2}} \tag{2.21}$$

Note that if the plasma is transparent (no absorption takes place) and the laser flux does not change with time

$$\phi_L \cdot r^a = \text{const} . \tag{2.22}$$

The ionization and recombination rate equations can be similarly reduced.

## II/2. Discretization

Only the main features of the discretization procedure used shall be outlined here.

An explicite difference scheme, centered both in space and time (second order accuracy) was used for solving

all basic equations but the energy equation. The energy equation was linearized and solved implicitly (by a Gaussian reduction of the resulting three-diagonal matrix) for each time instant. In addition, the presence of the ionization source term in the energy equation (with temperature-dependent rate coefficients) made it necessary to apply a predictor-corrector-type procedure at that point. The time increment was preselected for each time-step in accordance with the Courant-Friedrichs condition [16], and, if necessary, was adjusted (i.e. reduced) subsequently by checking the relative change of the basic variables.

In discretizing the energy equation (2.16)

$$\frac{e^{n+1}_{j+1/2} - e^{n}_{j+1/2}}{\Delta t} = -(\gamma-1)\, p^{n+1/2}_{j+1/2}\, \frac{V^{n+1}_{j+1/2} - V^{n}_{j+1/2}}{\Delta t} + \cdots$$

the pressure appearing in the first term on the right side is unknown to times $n+1/2$ (the sequence of time levels are denoted by the upper index "n" and the sequence of the Lagreangean cell boundaries by the lower index "j". Hence in a centered difference scheme index "n + 1/2" denotes the mid-time between the time levels n and n+1, and "j + 1/2" denotes the cell bounded by the shells j and j + 1).

The pressure $p^{n+1/2}_{j+1/2}$ can be expressed, however, by means of a series expansion around the time $t_n$:

$$p^{n+1/2} = p^{n} + \frac{\partial p}{\partial e}\Big)^{n}\left(e^{n+1/2} - e^{n}\right) + \frac{\partial p}{\partial V}\Big)^{n}\left(V^{n+1/2} - V^{n}\right) + \cdots$$

Assuming $e^{n+1/2} - e^{n} \approx \frac{1}{2}\left(e^{n+1} - e^{n}\right)$; $V^{n+1/2} - V^{n} \approx \frac{1}{2}\left(V^{n+1} - V^{n}\right)$ and using the ideal gas state equation we obtain

$$p^{n+1/2} \approx p^{n}\left[1 - \tfrac{1}{2}\left(V^{*} - 1\right) + \tfrac{1}{4}\left(V^{*} - 1\right)^{2} + \cdots\right]$$

where $V^{*} = V^{n+1}/V^{n}$ represents a local "compression ratio".

Furthermore, the product $(e^{5/2}\partial e/\partial\psi)^{n+1/2}$ appearing in the fourth term of the discretized version of eq. (2.16) was linearized by assuming $|(e^{n+1}-e^n)/e^n|<1$ and applying a binomial expansion. The above product is thus replaced by the following expression:

$$\tfrac{1}{2}(e^n)^{3/2}\left[2e^{n+1}\left(\frac{\partial e}{\partial\psi}\right)^n+e^n\left(\frac{\partial e}{\partial\psi}\right)^{n+1}-e^n\left(\frac{\partial e}{\partial\psi}\right)^n\right]$$

One will note that $e^{n+1}$ is linear in this expression.

## III. RESULTS

Computations were performed for two wavelengths: $\lambda = 1.06\,\mu$ (Nd-glass laser) and $\lambda = 10.6\,\mu$ ($CO_2$ gas laser). In both cases, a rectangular laser pulse ($\phi=\phi_0=$ const for $0\le\tau\le\tau_{pulse}$, $\phi=0$ for $\tau<0$, $\tau>\tau_{pulse}$) was used. Other laser pulse shapes were tested as well, however, since the primary purpose of these calculations was a comparative study of the laser wavelength effects, no effort was made at pulse shape optimization. A 30 ns pulse duration was selected for the Nd laser and several pulse lengths (up to 1 $\mu$s) were tested for the $CO_2$ laser. In the case of plane targets the laser flux intensity was varied between $10^{12}$ and $10^{13}$ W/cm$^3$. The laser energy per target volume was of the order of $10^6$ to $10^7$ J/cm$^3$ in all cases considered.

For ensuring equivalent initial conditions for both wavelengths, a low density high-temperature plasma sheath was assumed to envelop the cold core on the side of the incident beam (see Fig. 2). The linear dimension of this layer was chosen equal to the pellet dimension (pellet radius) and the gas density was assumed to very linearly in the sheath from zero (at the outer boundary) to the critical (cut-off) density value at the sheath-solid interface.

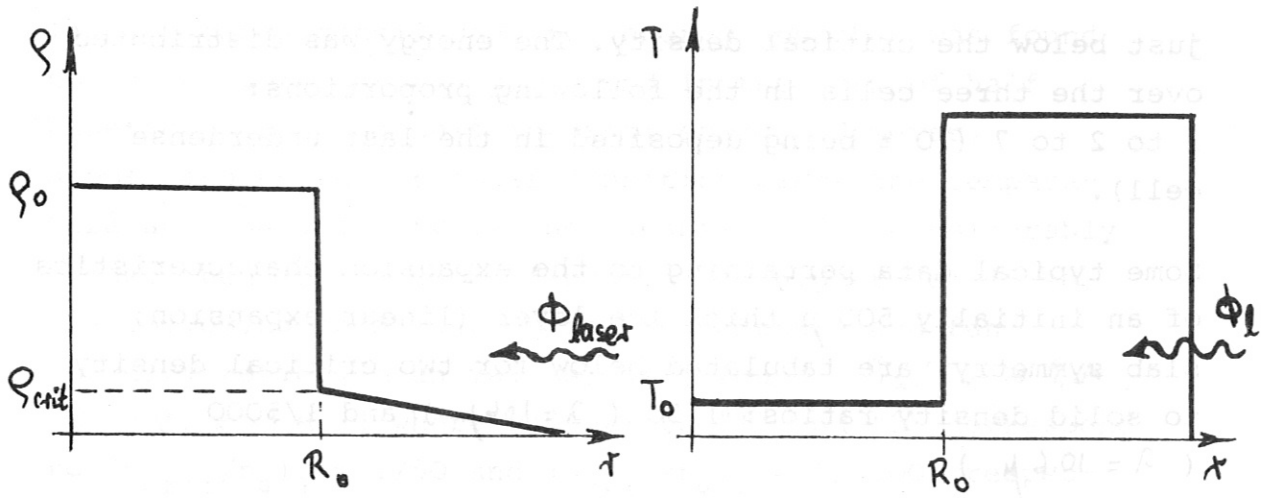


Fig. 2. Assumed initial parameter distributions

The temperature of the sheath was assumed to be approx. 2 eV. The resulting initial electron densities combined with the given absorption path (sheath thickness) were sufficient to initiate effective initial absorption. Since the energy stored in the rather low-density absorbing sheath ( $\rho_{crit}/\rho_0$ = 1/50 and 1/5000 for $\lambda = 1.06\mu$ and $\lambda = 10.6\mu$ , respectively) is negligible compared with the energy supplied by the laser to the target, its effect on the expansion dynamics and the overall heating efficiency already becomes negligible in the early phase of plasma expansion.

## III/1 Effect of laser wavelength on absorption and expansion characteristics in the case of anomalous absorption (100 % energy deposition at critical density)

For simulating anomalous absorption processes which may result in energy deposition rates significantly exceeding the values predicted by inverse bremsstrahlung (see, for example, Galeev and Sagdeev [17] for parametric decay instability), it was assumed in a series of calculations that the low-density fan of the expanding plasma is fully ionized and the laser beam energy is completely absorbed in the last three mass-cells with densities

just below the critical density. The energy was distributed over the three cells in the following proportions: 1 to 2 to 7 (70 % being deposited in the last underdense cell).

Some typical data pertaining to the expansion characteristics of an initially 500 $\mu$ thick ice layer (linear expansion, slab symmetry) are tabulated below for two critical density to solid density ratios: 1/50 ( $\lambda = 1.06\,\mu$ ) and 1/5000 ( $\lambda = 10.6\,\mu$ ).

Table 1 PLASMA CHARACTERISTICS AT THE END OF THE LASER PULSE. EXPANSION IN VACUUM, SLAB SYMMETRY, 270 J LASER ENERGY, TOTAL ABSORPTION AT THE CRITICAL DENSITY ($\phi_L \approx_{pulse} = 1.08 \times 10^5$ J/cm$^3$)

a) $n_{cr}/n_o$ = 1/50 30 ns pulse duration

b) $n_{cr}/n_o$ = 1/5000, 30 ns " "

c) $n_{cr}/n_o$ = 1/5000, 120 ns " "

| A. PLASMA COORDINATES | INITIAL COORD. (cm) | (a) | (b) | (c) |
|---|---|---|---|---|
| IRRADIATED (HOT-END) VACUUM BOUNDARY (cm) | 0.05 | 5.3 | 8.8 | 40.0 |
| HOT-SIDE CORE BOUNDARY (INITIALLY ICE-PLASMA INTERFACE) (cm) | 0.0 | 1.2 | 2.2 | 9.0 |
| CRITICAL DENSITY LAYER (cm) | 0.0 | 0.0 | 2.2 | 9.0 |
| COLD-END VACUUM BOUNDARY (cm) | -0.05 | -0.13 | -0.13 | -0.4 |
| **B. FRACTIONAL ENERGY CONTENT** | | | | |
| KINETIC ENERGY | | 55 % | 54 % | 56 % |
| INTERNAL ENERGY | | 45 % | 46 % | 44 % |

In both cases considered, the energy absorbed was found to be recovered at the pulse end in the form of half kinetic energy and half internal energy. However, depositing energy at lower densities makes the temperature and the velocity of the expansion fan considerably higher then in the case of heating at higher densities. The following quantitative fan temperature and fan velocity ratios (mean values) were found: $T_2/T_1 \approx 2.4$, $v_2/v_1 \approx 1.5$, where subscripts "1" and "2" correspond to $(n_{crit}/n_0)_1 = 1/50$ and $(n_{crit}/n_0)_2 = 1/5000$, respectively. Comparing the expansion coordinate values tabulated one may note the significant difference between the data corresponding to the two different wavelengths. While in the case of the shorter wavelength the critical density locus penetrates into the initially cold high-density core material, when heating at a longer wavelength the coordinate of the critical density layer remains "attached" to the hot-side core boundary. Hence in this case the absorption layer could not penetrate the core during the laser pulse and the expanding high-density core simply sweeps in front of it a low-density high-temperature absorption fan. Longer expansion times and larger expansion distances are required for overcoming the 5000 to 1 density difference. As will be seen in the next section, this circumstance also has consequences when classical collisional absorption (inverse bremsstrahlung) is being considered.

A final note: The large expansion fan velocities and high temperatures found in heating at longer wavelengths, i.e. the production of energetic particles, is highly undesirable if filling of magnetic confinement configurations is considered. Flares of energetic particles may seriously impair the confinement characteristics and may thus be accompanied by significant particle losses.

III/2 Effect of laser wavelength on absorption and expansion characteristics in the case of classical absorption (inverse bremsstrahlung)

In this series of calculations, energy was deposited in the mass-cells in accordance with eqs. 2.20 and 2.21. The results may be summarized as follows:

a) Slab symmetry:

When an ice layer 500 $\mu$ thick was irradiated with a Nd glass laser (flux intensity up to $3.6 \times 10^{12}$ W/cm$^2$) pulse duration 30 ns) up to 80 % of the incident energy was absorbed. By the end of a 30 ns pulse approx. 10 % to 15 % of the 500 $\mu$ thick initially high-density ice core material is affected (heated) directly by inverse bremsstrahlung and a further 5 % to 10 % by the heat wave emerging from the absorption zone (at the relatively low laser flux intensities considered here, the heat wave lags behind the shock wave). The rest of the core material is only shock-heated and thus remains relatively cold. Only 10 % to 15 % of the mass succeeds in expanding down to the critical density value within the time of the laser pulse.

Irradiating the same ice layer (500 $\mu$ thick) with a $CO_2$ laser (pulse energy the same as above, pulse length 30 ns to 200 ns) only about 4 % of the incident energy was found to be absorbed. Higher absorption efficiencies - up to 26 % - could only be observed by heating rather thin ( 100 $\mu$) ice layers with long pulses. In this case the shock-heated target rapidly expands on both sides of the initially cold layer and part of the core material still has time to expand down to the critical density within the pulse duration.

The lower absorption efficiencies inherent in heating at longer wavelengths may be explained as follows: The energy absorbed by inverse bremsstrahlung is proportional (at best) to the local electron density, which has an upper limit defined by the critical (cut-off) density value. This upper limit is a factor of 100 lower for a $CO_2$ laser than for a Nd-glass laser. Furthermore, since the expansion fan is usually thinner and hotter if heated at longer wavelengths (energy is being deposited at lower mass-densities), the absorption becomes still less effective (the absorptivity is inversely proportional to $Te^{3/2}$). Of course, the energy absorbed could be increased by increasing the absorption length and thus balancing the lower absorptivity value. However, if filling of magnetic confinement machines with laser produced plasmas is considered and the multi-dimensionality of the problem (plasma expansion perpendicular to the laser beam direction) is not neglected, there are clear limitations on the maximum absorption lengths obtainable.

Some representative data pertaining to the expansion coordinates of plasmas heated at different wavelengths are given in Fig. 3 (compare also with the data given in Table 2 for 100 % absorption). The symbols $x_o$, $x_1$, $x_{defl}$, $x_e$ denote the coordinates of the hot-end vacuum boundary, the hot-side core boundary (initially plasma-ice interface), the deflagration zone boundary (coincides roughly with the absorption zone boundary), and the cold-end vacuum boundary, respectively.

b) Spherical symmetry:

The results obtained for the two different wavelengths are qualitatively the same as those obtained for slab symmetry: poor absorption at the longer wavelength and fairly good absorption at the shorter wavelength. The absorption efficiencies calculated are, in general, lower

ABSORPTION AND PLASMA EXPANSION AS FUNCTIONS OF WAVELENGTH.
SLAB MODEL: $\phi_L = 2.5 \times 10^{12}$ W/cm$^2$, $\tau_p = 30$ns(Nd)
$\phi_L = 0.62 \times 10^{12}$ W/cm$^2$, $\tau_p = 120$ns($CO_2$)
COLLISIONAL ABSORPTION.

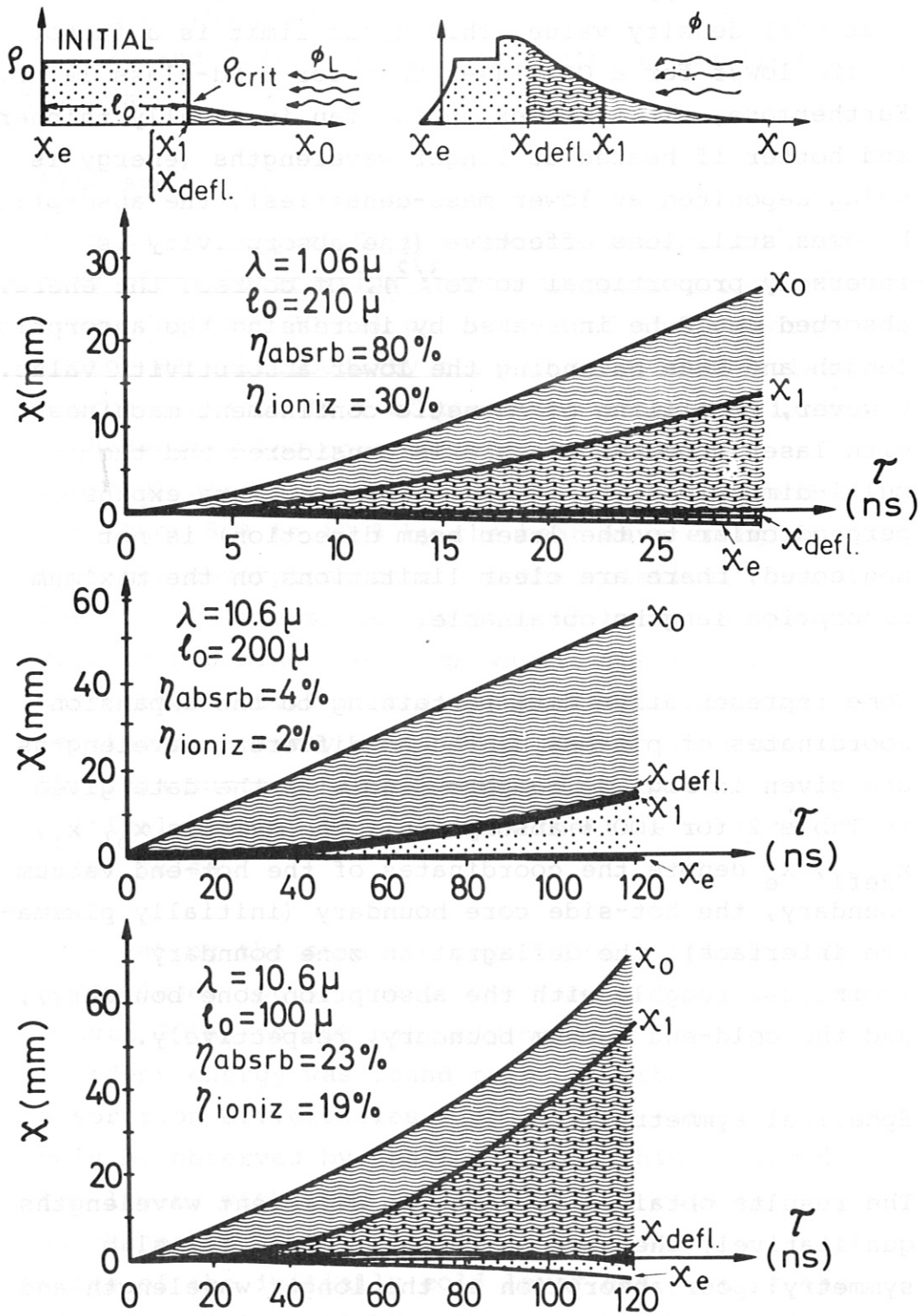


FIG.3

than those characterizing linear expansion, the difference being due to the specific (gasdynamic) characteristics of spherical expansion as compared with linear expansion. This question shall be considered further in the following section.

Typical data characterizing the time variation of the energy content (integral characteristics) of a spherically irradiated pellet are shown in Fig. 4 for a 100 J/30 ns laser pulse (Nd glass laser, expansion in vacuum). Inverse bremsstrahlung has been assumed here as absorption mechanism, and collisional and photo-processes define the respective ionization and recombination processes. As can be seen, in the early absorption phase ( $\tau < 200$ ps ) gasdynamic motion is still bound by inertia and all the energy absorbed reappears as internal energy. As the temperature (and pressure) rises, absorption becomes less efficient and, at the same time, rapid expansion sets in. In about 2 ns the kinetic energy of the expanding gas exceeds the energy fraction appearing as internal energy and the bulk temperature approaches a saturation value. By the end of the pulse about 47 % of the irradiated energy is absorbed and over 90 % of the energy absorbed appears as kinetic energy. The fraction of energy spent for ionizing the pellet material reaches its maximum at the pulse end: about 48 % of the mass is ionized by this time. After the pulse ends the plasma undergoes free expansion in vacuum characterized by a state of forzen equilibrium: rapidly decreasing bulk static temperature at almost constant ionization degree. Owing to the finite recombination rates and rather low gas densities, the bulk ionization degree does not change significantly within the first microsec. By this time, the absorbed energy is almost totally converted into kinetic energy.

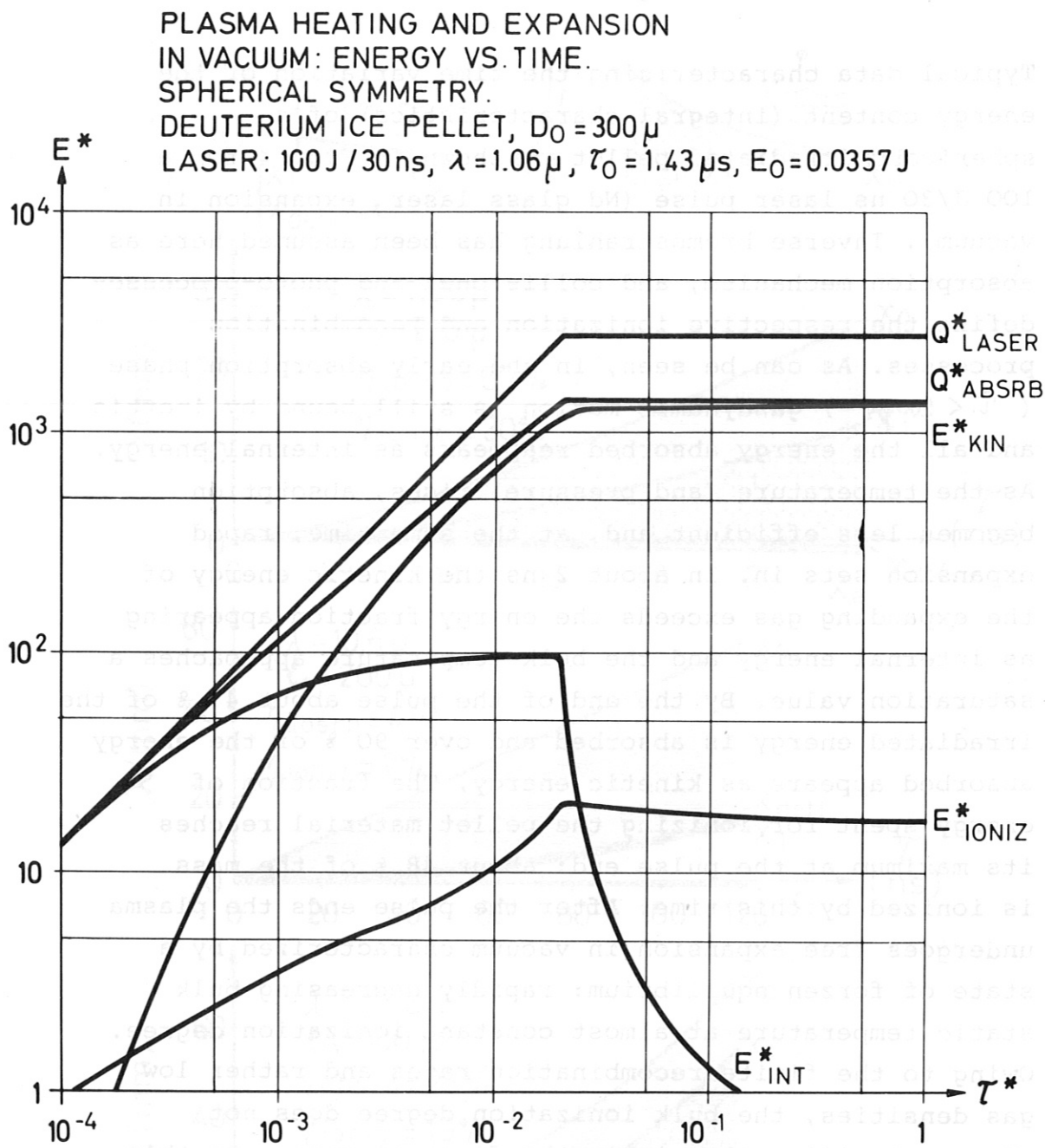
PLASMA HEATING AND EXPANSION
IN VACUUM: ENERGY VS. TIME.
SPHERICAL SYMMETRY.
DEUTERIUM ICE PELLET, $D_0 = 300\,\mu$
LASER: 100 J / 30 ns, $\lambda = 1.06\,\mu$, $\tau_0 = 1.43\,\mu$s, $E_0 = 0.0357$ J
E*
$10^4$
$10^3$
$10^2$
10
1
$10^{-4}$
$10^{-3}$
$10^{-2}$
$10^{-1}$
1
$\tau^*$
$Q^*_{LASER}$
$Q^*_{ABSRB}$
$E^*_{KIN}$
$E^*_{IONIZ}$
$E^*_{INT}$

FIG. 4

## III/3 Geometry effects on classical absorption

There are notable differences in the expansion dynamics of plasma configurations caused by differences in the symmetry properties of the models considered. If slab symmetry is assumed, the energy deposited in the absorbing layer produces a plane shock which propagates through the pellet heated. The plasma only expands against the laser beam as long as the pellet is not fully penetrated by the shock, and it expands to both sides for times exceeding the burn-through time (the pellet is of finite thickness). No reflected shocks are generated in this system and the density increase in the shocked material is limited by the classical Rankine-Hugoniot value. The rate of density change is characterized in this case by the linear dependence of the plasma volume on its linear dimension.

In the case of cylindrical and spherical symmetries the plasma expands against the incident laser beam all the time and strongly reflected shocks are produced at the symmetry center. The rate of density change during the expansion is characterized in this case by the quadratic (cylindrical) or cubic (spherical) dependence of the plasma volume upon its linear dimension.

The effect of the model symmetry assumed on the global absorption efficiency was found to be the same for both wavelengths considered: the absorption was found to be most efficient in the case of linear expansion (slab symmetry) and least favourable in the case of spherical expansion (central symmetry). The explanation of the phenomenon is straight-forward: If linear expansion is considered, the electron density decrease associated with the volumetric dilution of the plasma is smaller than that associated with spherical expansion.

The absorption integral (see eqs. 1.6 and 1.7) depends upon both the absolute value of the electron density (absorptivity) and the electron density gradient (thickness of the absorption zone). Since the electron density decreases much more rapidly during spherical expansion than during a linear process, the overall absorption efficiencies may differ by a factor of 1.6 to 2.0 for the two cases (for the same energy supplied per unit mass).

The spread in the factor values displayed above is due to the fact that - in the case of spherical symmetry - the absolute pellet size also affects the expansion process and the absorption efficiency.

For checking the effect of the pellet size on the absorption process and the global ionization degree obtainable, calculations were performed for a series of pellet sizes with diameters ranging from 180 $\mu$ to 500 $\mu$. The laser output characteristics were kept constant for these calculations: 100 J/30 ns at a wavelength $\lambda = 1.06\ \mu$. Spherical symmetry was assumed. Some instantaneous pellet/plasma properties corresponding to the pulse end ($\tau$ = 30 ns) are summarized for this case in Table 2.

Table 2 PELLET AND PLASMA PROPERTIES AT THE END OF THE LASER PULSE AS FUNCTIONS OF THE INITIAL PELLET SIZE. CLASSICAL ABSORPTION, EXPANSION IN VACUUM, SPHERICAL SYMMETRY, 100 J/30 ns LASER PULSE, $\lambda = 1.06\ \mu$.

| INITIAL DIA. ($\mu$) | 200 | 300 | 400 | 500 |
|---|---|---|---|---|
| TYPICAL CORONA TEMPERATURE (eV) | 15 | 12 | 12 | 11 |
| EXPANSION FAN VELOCITY (cm/sec) | $2.7 \times 10^7$ | $2.5 \times 10^7$ | $2.4 \times 10^7$ | $2.4 \times 10^7$ |
| PLASMA DIA. (cm) | 1.79 | 1.58 | 1.38 | 1.30 |

As can be seen, owing to the larger mass in the absorption fan of larger pellets the temperature decreases in the corona with increasing pellet size (for given initial corona radius to pellet radius ratio). The expansion velocity (and thus the plasma radius) also decreases with increasing pellet mass. Owing to the lower corona temperatures the absorption efficiency increases with increasing pellet size.

The effect of the pellet size on the overall heating efficiency is shown in Fig. 5. As can be seen, the fraction of the laser energy absorbed increases from approx. 30 % at $D_o$ = 200 $\mu$ to about 70 % at $D_o$ = 500 $\mu$. At the same time, because of the lower temperatures inherent in pellets with larger masses, the fraction of the total number of particles ionized (bulk ionization degree) decreases. However, the total number of ions produced increases with increasing absorption efficiency, i.e. with increasing pellet size. The variation of the maximum plasma radius and the core radius with the pellet size is also shown in Fig. 5 (core radius is defined as the radius of the material initially at ice temperature, i.e. $R_{core}(\tau = 0) = D_o/2$).

Hence by selecting larger pellets one could obtain better absorption efficiency, a larger number of ions, but, at the same time, also a larger number of cold neutral gas particles. If smaller pellets are used, the absorption process becomes less efficient, a smaller number of ions is produced but the pellet material becomes fully ionized.

Of course, effects not accounted for in this spherical symmetry approximation may quantitatively change the results presented here.

EFFICIENCY OF PELLET HEATING AS FUNCTION OF PELLET DIMENSION.
LASER: 100 J/30 ns, $\lambda = 1.06\mu$.
SPHERICAL SYMMETRY, EXPANSION IN VACUUM.

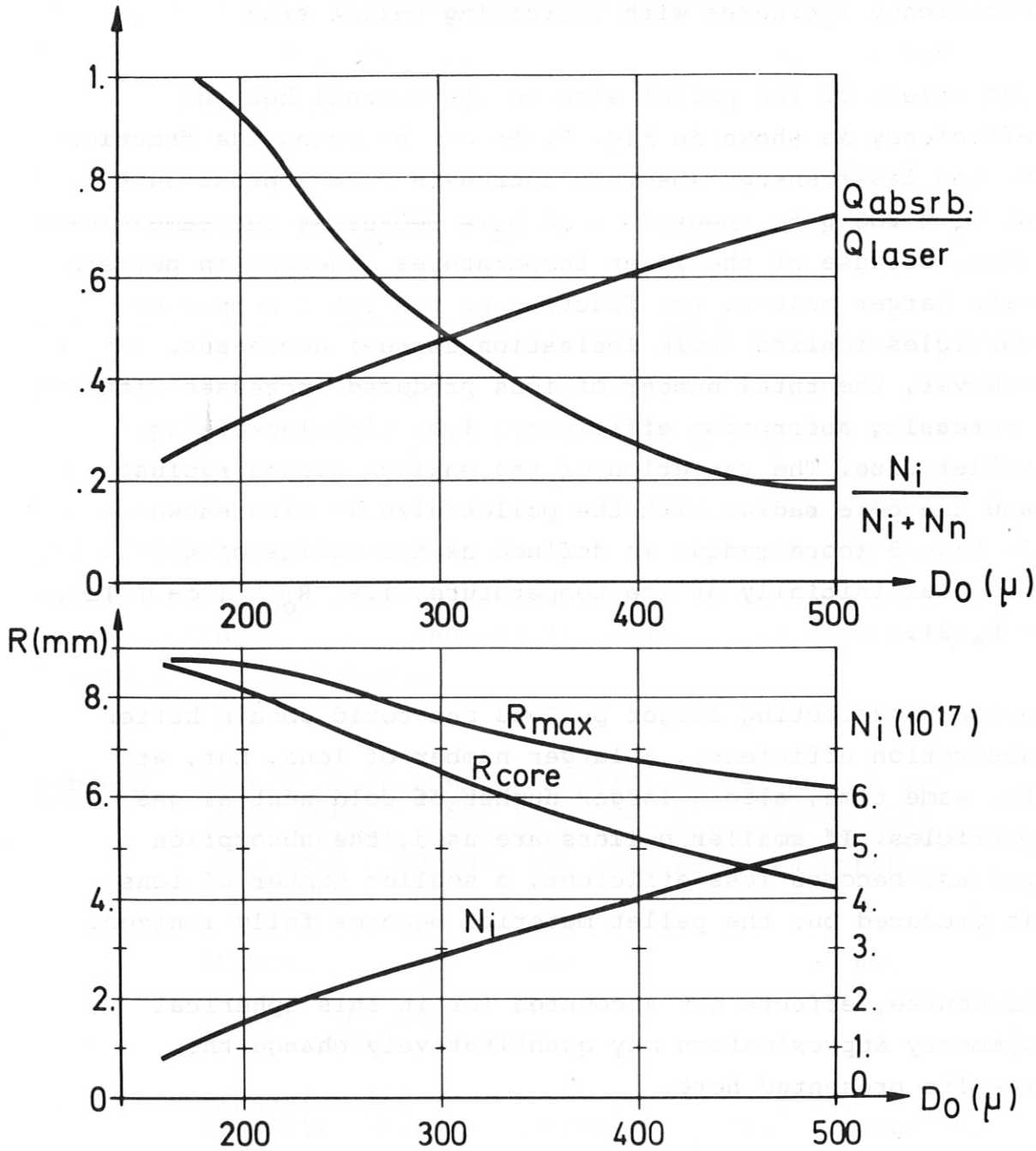


FIG. 5

It is of interest to note that allowance for ionization by electron impact and thermal radiation decouples the absorption layer ( $n_e = n_{crit}$ ) from the ionization front. Owing to shock heating and thermal conduction effects the material on the high-density side of the critical-density layer may become partially ionized before becoming directly exposed to laser light. (Part of the material heated may never be directly affected by the laser light). Furthermore, if the absorption layer passes through a region of steep positive density gradient, the layer may remain partially ionized for times defined by the respective relaxation times and may thus also be decoupled from the gas layer in which the neutral particle density is equal to the critical density ($n_n = n_{crit}$ ). For times not exceeding the pulse duration the distance between the $n_e = n_{crit}$ and the $n_n = n_{crit}$ layers was found to be within the dimensions of one or two mass cells. (A mass cell represents in this case the maximum resolution of the numerical system employed). For times exceeding the laser pulse duration the critical electron density layer becomes completely decoupled from the respective neutral particle density layer because of the difference between the gasdynamic and recombination relaxation times. The gasdynamic rarefaction wave that propagates towards the pellet center lags considerably behind the "electron rarefaction" wave, which also converges to the pellet center. The rapid electron density decrease is caused by the simultaneous volumetric dilution and recombination processes. (Note, however, that the ionization degree is governed by the rate of recombination alone.) Hence, if the expansion is not disturbed by external means (by the presence of a magnetic field, for example), the electron density decreases more rapidly than the gas density. This should be kept in mind when the possible application, timing, and optimization of a second laser pulse are considered. A second pulse may be found useful for fully ionizing the partially ionized expanding target-plasma and heating it to a given temperature.

## III/4 Spherical expansion in a magnetic field

In the last series of calculations, the effect of a magnetic field on spherical plasma expansion was considered. Computations were performed for two different wavelengths; however, the absorption efficiency and expansion dynamics characterizing the different wavelengths were found to be the same as those reported in Sect. III/2.

Typical time-variations of the pellet energy content are shown in Fig. 6 for Nd-glass laser wavelength and a magnetic field strength of 1 Tesla. The diamagnetic approximation described in Sect. I/5 was used in computing the effect of the magnetic field on the plasma expansion. As can be seen, for times not exceeding approx. 30 ns (equal in this case to the pulse duration), i.e. for times during which the plasma pressure at the outer boundary of the expanding plasma blob exceeds significantly the magnetic field pressure, the diamagnetic work remains negligible and the time variation of the various energy forms (kinetic, internal, ionizational) remains essentially the same as that seen in the case of vacuum expansion (compare Fig. 6 with Fig. 4).

After approx. 50 ns the magnetic field effect becomes apparent: After reaching a minimum at approx 60 ns the bulk pellet temperature starts to rise and the kinetic energy content to decrease rapidly. The outer plasma boundary comes to a full stop in approx. 200 ns, most of the energy being stored at this moment in flow work spent for stretching the magnetic field lines (there is still some plasma motion inside the sphere). This energy is then recovered during the following contraction of the magnetic field lines and the accompanying spherical compression of the confined plasma blob. However, since in a practical magnetic field configuration the plasma

PLASMA HEATING AND EXPANSION IN MAGNETIC FIELD: ENERGY VS. TIME. SPHERICAL SYMMETRY. DEUTERIUM ICE PELLET, $D_0 = 300\,\mu$, $B_0 = 1$ TESL. LASER: 100 J / 30ns, $\lambda = 1.06\,\mu$. REF. QUANTITIES: $\tau_0 = 1.46\,\mu s$, $E_0 = 4\pi\ Q_0 = 0.0357$ J.

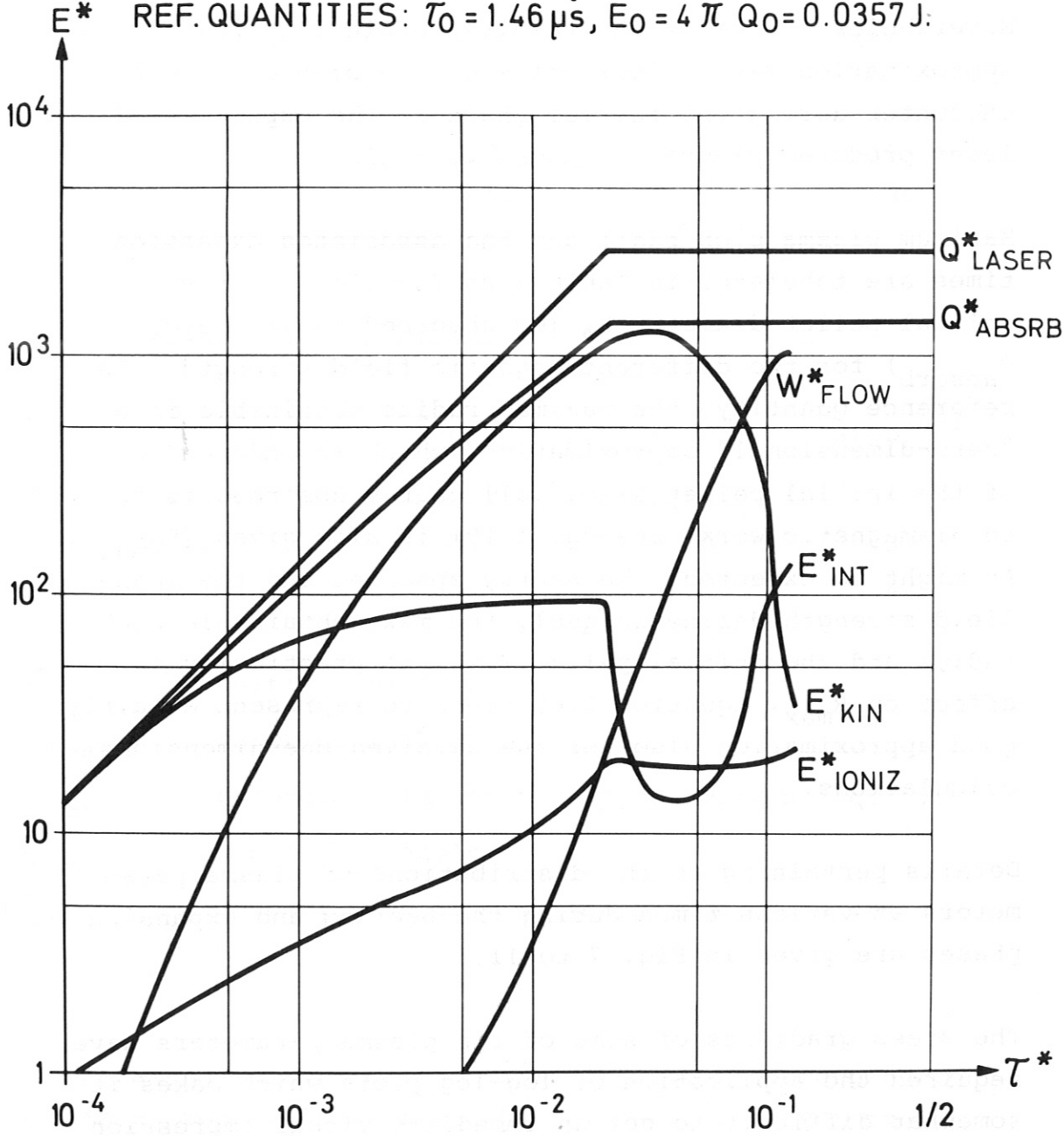


FIG. 6

starts to escape along the magnetic field lines long before the full stop of the boundary is indicated by this diamagnetic approximation, the present results can only be used for estimating the maximum radius the plasma blob may achieve in the transverse direction and the expansion time associated with this maximum radius. Nevertheless, some of the results obtained in this approximation may be indicative of the problems one may encounter during the initial phase of the expansion of laser produced plasmas in magnetic fields.

Maximum plasma blob radii and the associated expansion times are tabulated in Table 3 as functions of the initial pellet diameter $D_o$ (or absorbed laser energy $Q_{absorb}$) for two different magnetic field strengths. As reference quantity, the maximum radius obtainable in a "zero-dimensional" approximation, which is independent of the initial pellet size, (all energy absorbed is spent on diamagnetic work; see eq. 1.19) is also given ($R_{O_{max}}$). As might be expected, the energy absorbed and the magnetic field strength define uniquely the max. obtainable blob radius and the initial pellet size has practically no effect on $R_{max}$. Equation 1.19 seems to represent a fairly good approximation also for the detailed one-dimensional calculations.

Details pertaining to the distributions of plasma parameters at various times during the heating and expansion phases are given in Fig. 7 to 11.

The steep gradients of some of the plasma parameters have required the application of log-log plots which makes it somewhat difficult to get an immediate visual impression of the true (linear scale) spatial distributions.

Table 3 MAXIMUM PLASMA RADIUS TRANSVERSE TO THE MAGNETIC FIELD

$B_o$ = 1 tesla

| $D_o$ (μ) | $Q_{absorb.}$ (J) | $R_{o_{max}}$ (cm) | $R_{max}$ (cm) | $\tilde{\tau}_{stop}$ (ns) |
|---|---|---|---|---|
| 250 | 43.5 | 2.96 | 2.85 | 171 |
| 300 | 47.2 | 3.04 | 2.90 | 175 |
| 500 | 73.0 | 3.52 | 3.13 | 230 |

$B_o$ = 0.5 tesla

| $D_o$ (μ) | $Q_{absorb.}$ (J) | $R_{o_{max}}$ (cm) | $R_{max}$ (cm) | $\tilde{\tau}_{stop}$ (ns) |
|---|---|---|---|---|
| 250 | 43.9 | 4.71 | 4.59 | 262 |
| 300 | 51.6 | 4.97 | 4.60 | 280 |
| 500 | 75.0 | 5.64 | 5.30 | 320 |

$D_o$ - initial pellet size

$Q_{absorb.}$ - absorbed energy calculated

$R_{o_{max}}$ - zero-dim. diamagnetic approximation (eq. 1.19)

$R_{max}$ - numerical result

$\tilde{\tau}_{stop}$ - deceleration time of the plasma boundary

The parameter distributions shown in Fig. 7 correspond to a time approx. 2.3 ns after the pulse-start. A strong shock wave driven by a rapidly expanding plasma fan converges to the center of the pellet. Note that "-v" and "+v" denote inwardly and outwardly directed radial flow velocities, respectively. The pressure and temperature change acorss the shock by more than three and four orders of magnitude, respectively. (Note, however, that $T/T_o \approx 10^3$ has been specified as initial condition for the absorption fan).

The degree of ionization approaches unity in the high temperature expansion fan, but it falls rapidly to negligible values in the purely shock-heated high-density zone.

Figures 8 and 9 correspond to a state after the central reflection of the spherically converging shock: $\tilde{\tau} \approx 10$ ns. The shock now runs outward into a still inwardly moving and relatively cold, purely shock-heated high-density gas region. The gas behind the reflected shock (in the pellet center) is partially ionized, but the degree of ionization drops to rather low values in the still inwardly moving and not absorbing high-density region. It rises to unity in the absorbing and rapidly expanding corona. Note the differences between the scales of these two figures and the previous one.

Finally, Fig. 10 and 11 represent plasma parameter distributions relatively long after the pulse end: $\tilde{\tau} \approx 105$ ns. The bulk of the plasma is in a state of uniform expansion: the pressure decreases and the velocity increases linearly with radius. The temperature is still constant over a large portion of the pellet mass. The narrow temperature dip (log-scale) in the central region is due to the fact that this region was never affected directly by radiation. The plasma radius is approx. 2 cm at this time, and about 45 % of the total mass is in the ionized state.

One will note the formation of a high-temperature high-density fully ionized plasma sheath at the outer plasma boundary caused by the decelerating effect of the magnetic field. In time this sheath produces an inwardly running shock followed by contraction (compression) of the entire plasma volume and by complete ionization of the entire pellet mass. However, how effective this secondary shock heating and ionization may be in a real situation cannot be found from the present one-dimensional approximation.

PLASMA PARAMETER DISTRIBUTIONS DURING SPHERICAL EXPANSION IN A MAGNETIC FIELD. $\tau^* = 1.6 \times 10^{-3}$ DEUTERIUM ICE PELLET. $D_0 = 300\,\mu$, $B_0 = 1$ TESL. LASER: 100 J / 30 ns, $\lambda = 1.06\,\mu$. REF. QUANTITIES: $\ell_0 = 500\,\mu$, $T_0 = 18.7°K$, $n_0 = 4 \times 10^{22}\,cm^{-3}$, $\tau_0 = 1.46\,\mu s$.

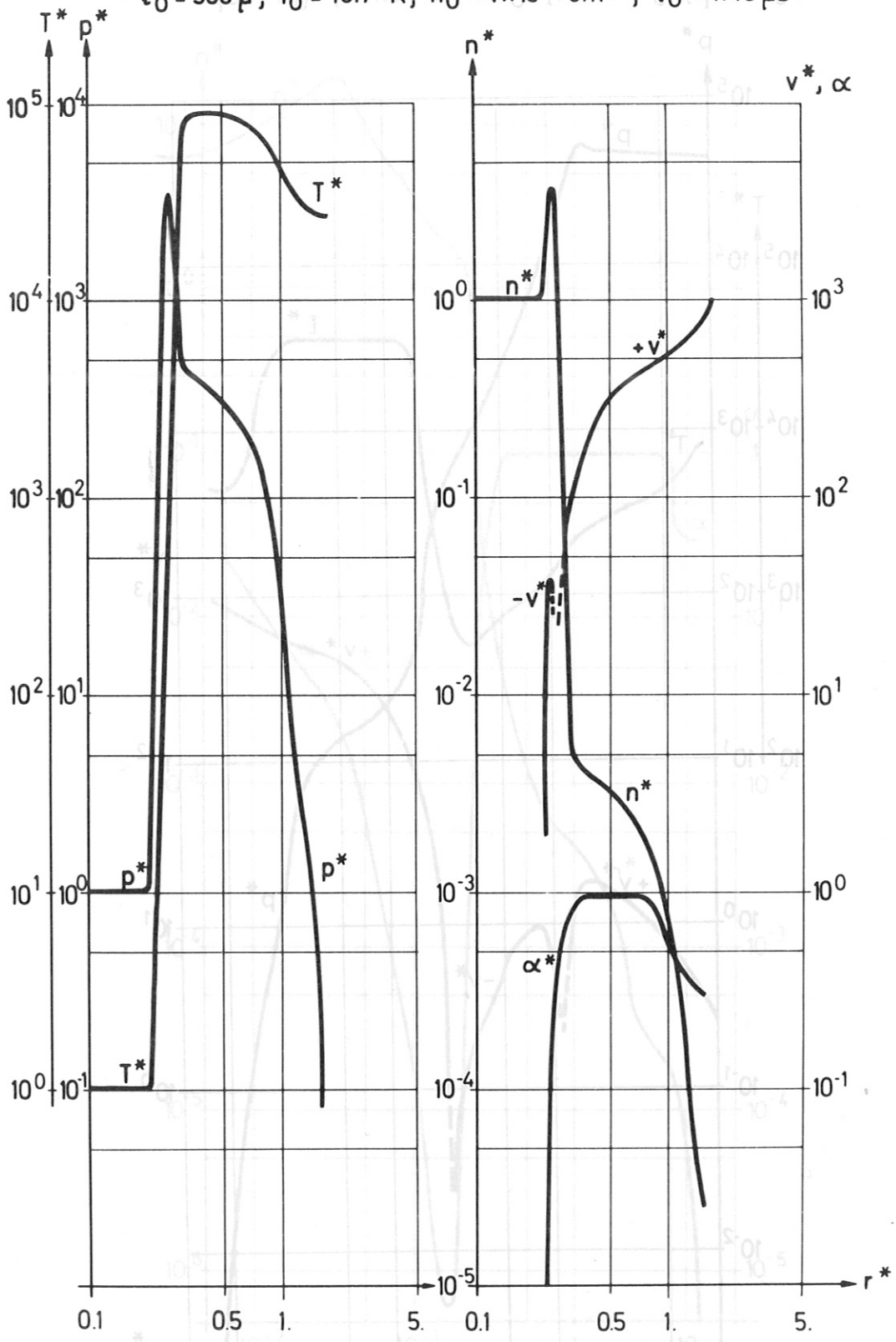


FIG. 7

PLASMA PARAMETER DISTRIBUTIONS DURING SPHERICAL EXPANSION IN A MAGNETIC FIELD. $\tau^* = 6.5 \times 10^{-3}$ DEUTERIUM ICE PELLET. $D_0 = 300\,\mu$, $B_0 = 1$ TESL. LASER: 100 J / 30 ns, $\lambda = 1.06\,\mu$. REF. QUANTITIES: $\ell_0 = 500\,\mu$, $T_0 = 18.7\,°K$, $n_0 = 4 \times 10^{22}\,cm^{-3}$, $\tau_0 = 1.46\,\mu s$.

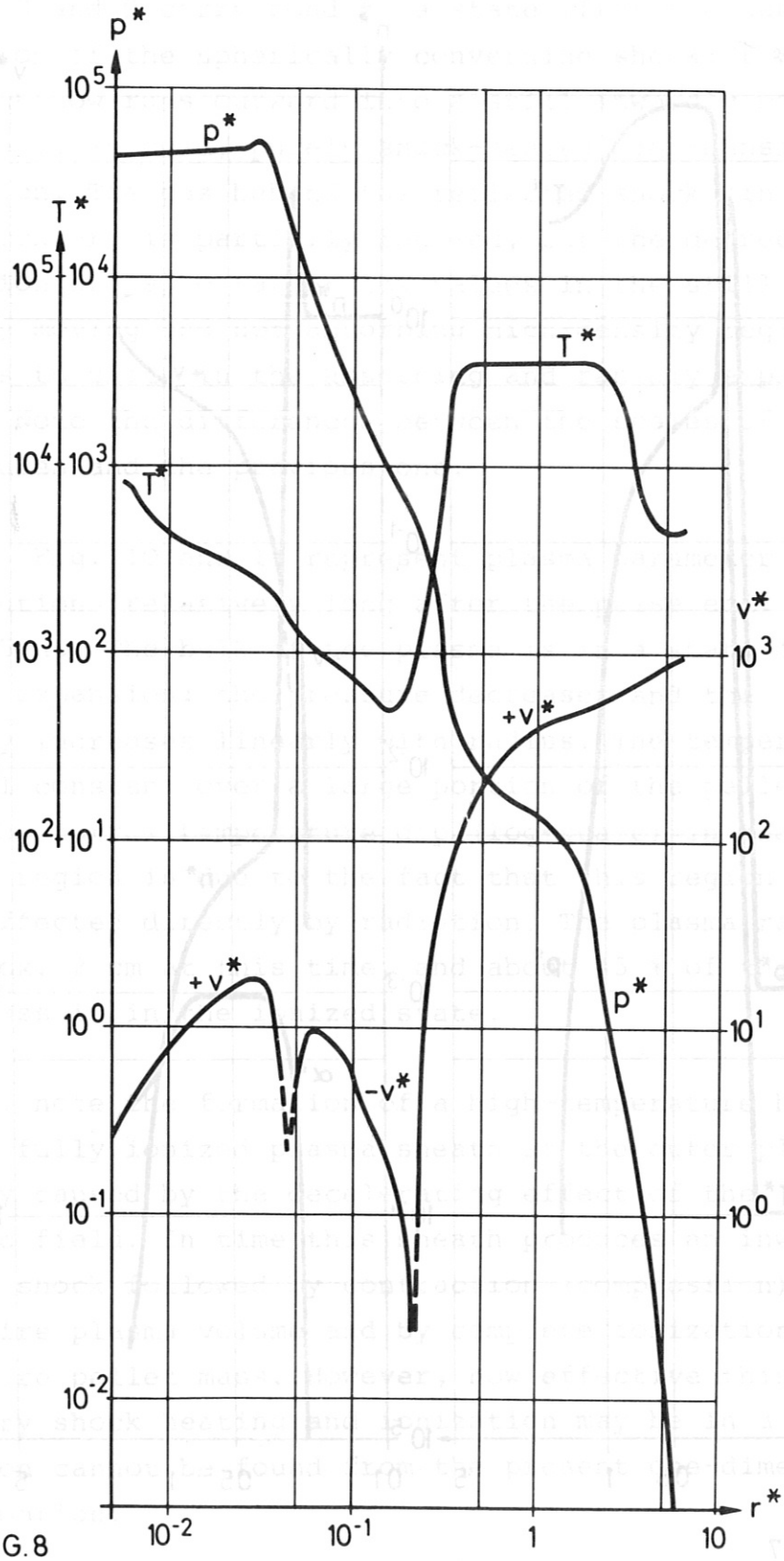


FIG. 8

PLASMA PARAMETER DISTRIBUTIONS DURING SPHERICAL EXPANSION IN A MAGNETIC FIELD. $\tau^* = 6.5 \times 10^{-3}$ DEUTERIUM ICE PELLET. $D_0 = 300\,\mu$, $B_0 = 1$ TESL. LASER: 100 J / 30 ns, $\lambda = 1.06\,\mu$. REF. QUANTITIES: $\ell_0 = 500\,\mu$, $T_0 = 18.7\,°K$, $n_0 = 4 \times 10^{22}\,cm^{-3}$, $\tau_0 = 1.46\,\mu s$.

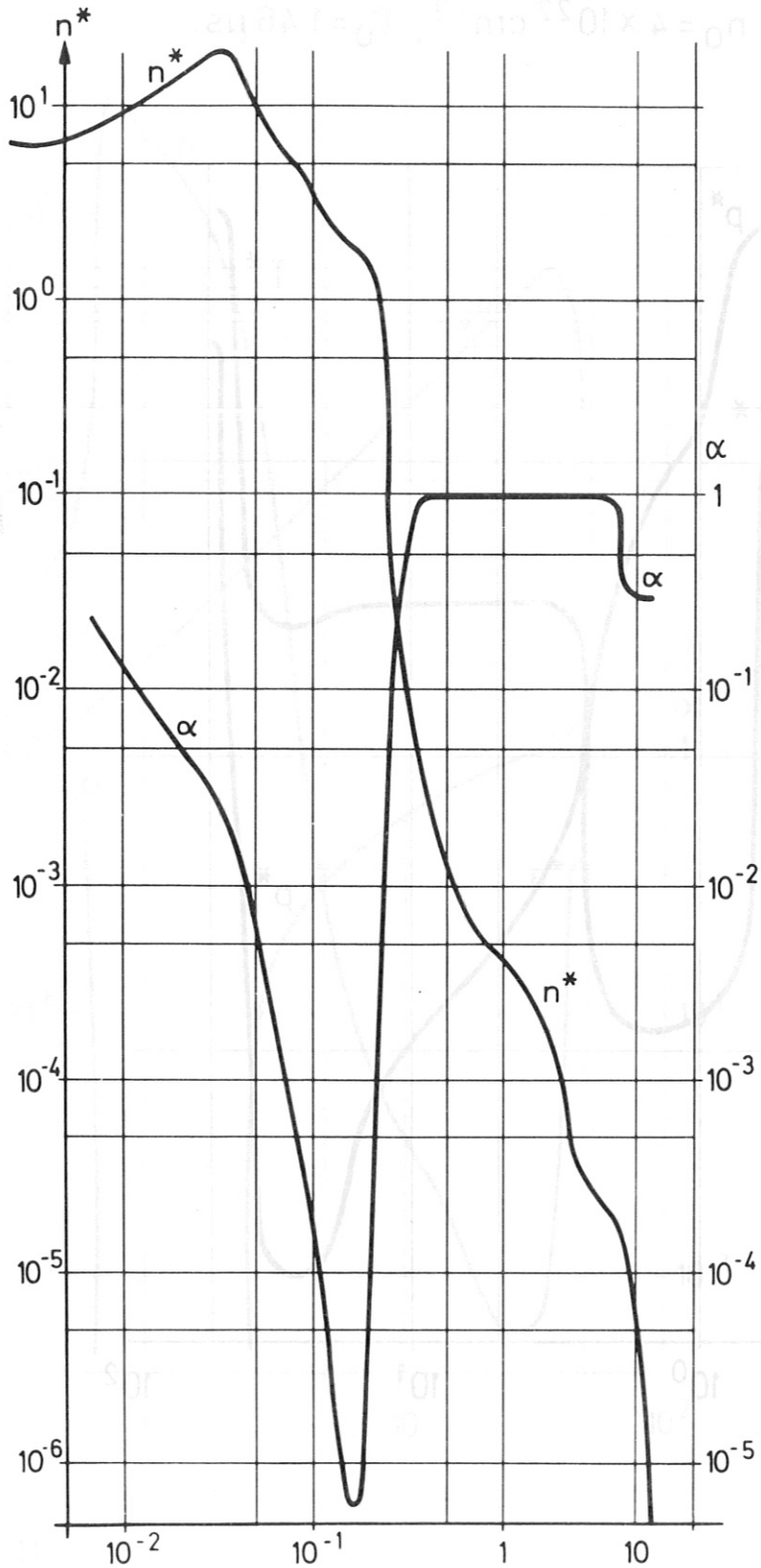


FIG.9

PLASMA PARAMETER DISTRIBUTIONS DURING SPHERICAL EXPANSION IN A MAGNETIC FIELD. $\tau^* = 7.3 \times 10^{-2}$. DEUTERIUM ICE PELLET. $D_0 = 300\,\mu$, $B_0 = 1$ TESL. LASER: 100 J/30 ns, $\lambda = 1.06\,\mu$. REF. QUANTITIES: $\ell_0 = 500\,\mu$, $T_0 = 18.7\,°K$, $n_0 = 4 \times 10^{22}\,cm^{-3}$, $\tau_0 = 1.46\,\mu s$.

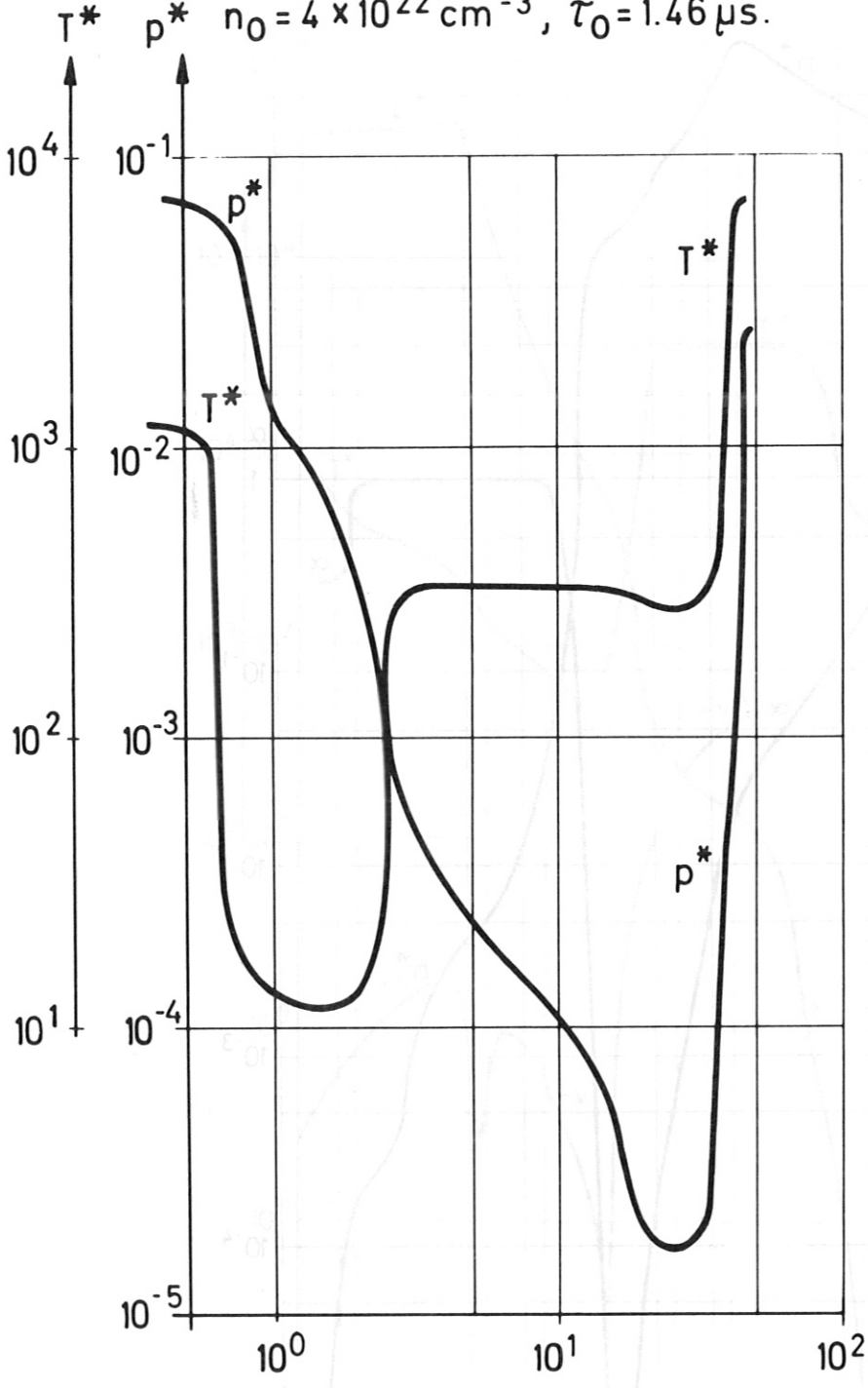


FIG. 10

PLASMA PARAMETER DISTRIBUTIONS DURING SPHERICAL EXPANSION IN A MAGNETIC FIELD. $\tau^* = 7.3 \times 10^{-2}$ DEUTERIUM ICE PELLET. $D_0 = 300\,\mu$, $B_0 = 1$ TESL LASER: 100 J/30 ns, $\lambda = 1.06\,\mu$. REF. QUANTITIES: $\ell_0 = 500\,\mu$, $T_0 = 18.7°K$, $n_0 = 4 \times 10^{22}\,cm^{-3}$, $\tau_0 = 1.46\,\mu s$.

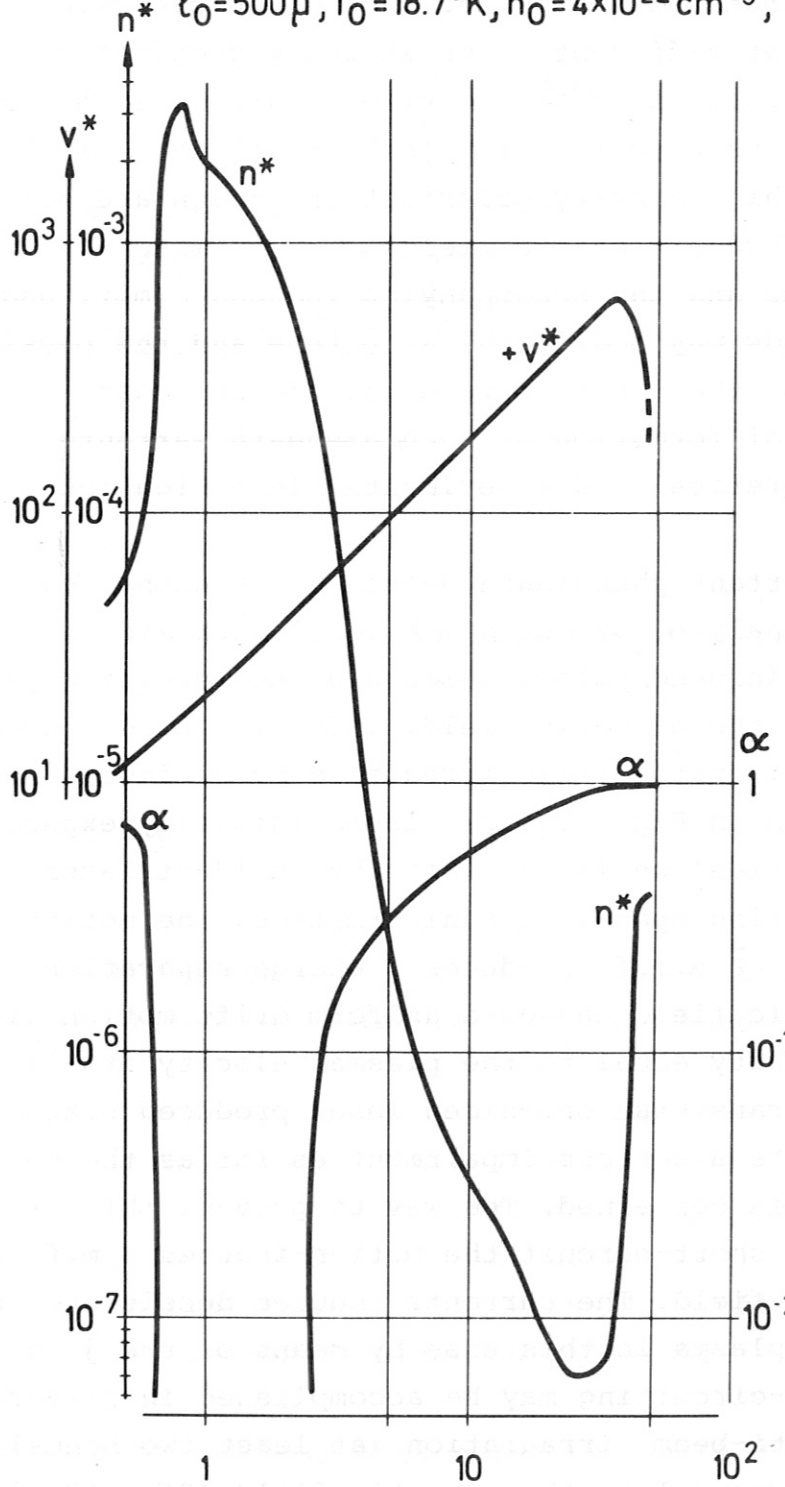


FIG. 11

An interesting aspect of the plasma expansion in a magnetic field that can be predicted from the last two figures is the possible presence of a strong electric field in this high-temperature outer sheath. Because of the difference of the electron and ion masses the two species are decelerated at different rates at the magnetic field-plasma interface, thus giving rise to strong local charge separation. The practical implications of this high-temperature high-density polarization sheath are not yet clear. Of course, magnetic field diffusion into the moving plasma and the accompanying induced e.m.f. and current fields may modify the structure and the physical properties of the sheath considered. In any case, the possibility of formation of such a sheath warrants further theoretical and experimental investigations.

Another important phenomenon whose effect cannot be adequately analyzed by one-dimensional approximations is e.m.f. - induced polarization and the resulting plasma drift across the magnetic field. Indeed, considering a target in a magnetic field irradiated by a single laser beam as shown in Fig. 12, the plasma initially expands almost one-dimensionally against the incident laser beam. Neglecting spatial nonuniformities, the motion induced $\vec{v} \times \vec{B}$ e.m.f. produces a charge separation whose electric field causes a uniform drift motion with a drift velocity equal to the plasma velocity itself. Hence this transverse one-sided laser produced plasma flare may constitute a serious impairment as far as the magnetic confinement is concerned. The way to prevent this drift motion is to short-circuit the motion-induced e.m.f. or polarization field. The currents induced decelerate and confine the plasma in this case by means of the $\vec{j} \times \vec{B}$ force. Short-circuiting may be accomplished in different ways: a) multi-beam irradiation (at least two beams) in the plane normal to the magnetic field (Fig. 12.a), b) single beam irradiation parallel to the magnetic field direction (axially symmetric plasma expansion; see Fig. 12.b), c) provision for a low-density fully ionized

background plasma in the magnetic volume where the target is to be irradiated; d) a combination of the above means.

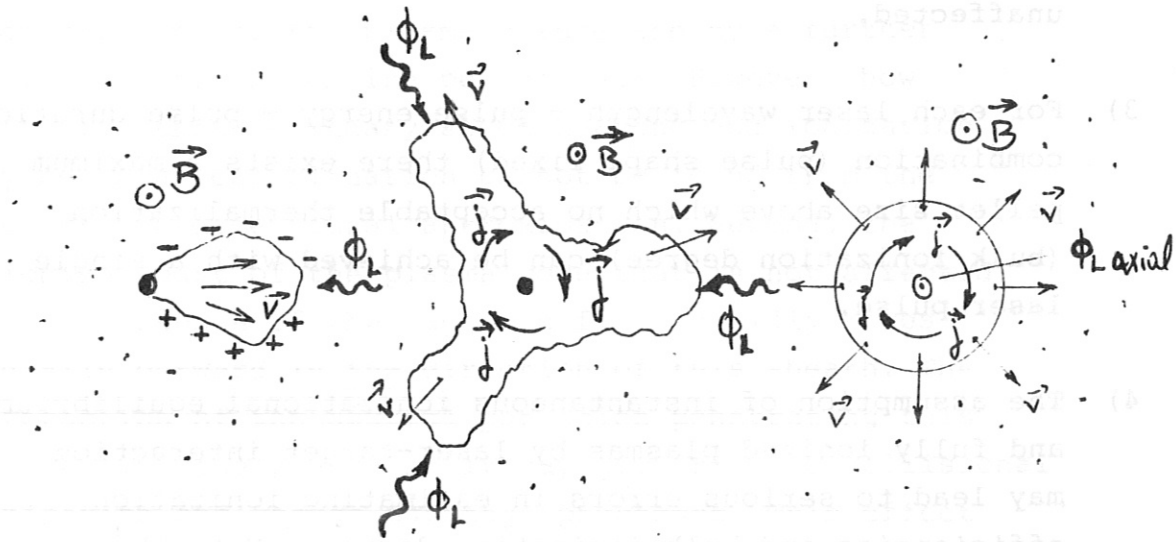


Fig. 12 Fig. 12.a Fig. 12.b

E.M.F.-induced drift and some ways of preventing it.
a) multi-beam irradiation in the plane normal to $\vec{B}$
b) Single-beam irradiation parallel to $\vec{B}$

## IV. SUMMARY AND CONCLUSIONS

Within the framework of the present approximation (see Sect. I) the following results have been obtained:

1) If inverse bremsstrahlung is considered as absorption mechanism, heating of the pellet core and ionization of the pellet mass are more effective at shorter wavelengths. The closer the critical (cutoff) density is to the initial target density the more effective are the absorption and ionization processes.

2) Even if anomalously high absorption (100 % energy deposition) is assumed at the critical density, i.e. equal absorption efficiencies for all wavelengths, the ionization process is still more effective at shorter wavelengths because of the more uniform plasma parameter distributions characterizing heating

at shorter wavelengths. Lasers with longer wavelengths produce hot and rapidly expanding plasma corona but leave the core of large-size pellets practically unaffected.

3) For each laser wavelength - pulse energy - pulse duration combination (pulse shape fixed) there exists a maximum pellet size above which no acceptable thermalization (bulk ionization degree) can be achieved with a single laser pulse.

4) The assumption of instantaneous ionizational equilibrium and fully ionized plasmas by laser-target interaction may lead to serious errors in estimating ionization efficiencies and bulk ionization degrees. Note that in the case of collisional- and photo - ionization processes the ionization rate coefficients are inversely proportional to some power of the electron temperature. Note, furthermore, that there are some $T_e$-$n_e$ combinations (high electron temperature, low electron density as exists, for example, in the expansion fan) for which photon processes may dominate over the collisional ones. Classical absorption calculations where the electron density is set automatically equal to charge number times the neutral particle density (assumption of fully ionized state) may yield wrong results as far as the location of the critical density layer and the total amount of energy absorbed are concerned.

5) If the pellet core has already been ionized (by a properly selected short-wavelength laser pulse), the expanding plasma may also be further heated at longer wavelengths. Owing to the highly non-uniform plasma property distributions inherent in the expansion phase care should be exercised in timing and selecting the duration of the second and subsequent laser pulses.

6) The transverse deceleration of a laser-produced plasma blob in a magnetic field may lead to the formation of a high-density high-temperature boundary layer at the

plasma-vacuum interface. The presence of this sheath at the transverse plasma boundary may have some practical implications. First, in time this sheath produces an inwardly running shock followed by a radial contraction (compression) of the plasma volume and by a further ionization of the entire pellet mass. However, how effective this secondary shock heating and ionization may be in a real situation cannot be found from the present one-dimensional approximation. Second, the unionized part of the plasma core that is not affected by the presence of the magnetic field rapidly moves radially outward in the direction of this sheath. The interaction of the neutral particles penetrating this sheath with the plasma in it may give rise to collisional ionization and charge exchange processes. This effect again cannot be investigated in the frame-work of the present one-fluid approximation. Third, because of the difference of the electron and ion masses the two species are decelerated at different rates at the magnetic field-plasma interface, thus giving rise to strong local charge separation.

7) Polarization-induced plasma drift may impair plasma confinement when asymmetric irradiation is applied transversely to the magnetic field direction. The drift effect may be reduced or eliminated by multi-beam irradiation across the magnetic field or by single beam irradiation parallel to the magnetic field direction. The same result may probably be obtained by providing a background plasma which envelops the pellet and short-circuits any polarization field that may be produced.

ACKNOWLEDGEMENT

The author thanks Dr. M. Salvat for his valuable comments pertaining to this report.
Parts of the numerical code used in this study were developed by H. Gorenflo. His skillful assistance is hereby acknowledged.

REFERENCES

1. See, for example: A.F. Haught et al., Laser initiated target experiment (LITE). Fifth Conference on Plasma Physics and Controlled Nuclear Fusion Research, Tokyo, 1974, Paper No. D5-3

2. See, for example: O.A. Anderson et al., Plasma production and confinement in the Baseball II mirror experiment; Fifth Conf. on Pl. Phys. and Contr. Nucl. Fus. Res., Tokyo, 1974, Paper No. D5-3

3. G. Tonon, Study of the expansion of a plasma produced by the interaction of a laser beam with a solid target (in French), Ph. D. Thesis, University of Lyon, 1973

4. See, for example: I.J. Spalding, Laser plasma heating, Euratom Adivsory Group on Heating and Injection, Rept. No. EUR-FU74/AGHI10/R1, Febr. 1974

5. W.D. Friedman, Trapping studies of a laser produced plasma in a toroidal quadrupole magnetic field. Ph. D. Thesis, The University of Rochester, 1973

6. A. Kitsunezaki, M. Tanimoto, and T. Sekiguchi, Cusp confinement of high-beta plasmas produced by a laser pulse from a freely-falling deuterium ice pellet. Phys. of Fluids, Vol. 17, No. 10, pp 1895-1902, 1974

7. Ch. M. Scott, Stellarator confinement of laser produced plasma; Ph. D. Thesis, The University of Texas at Austin, USA

8. G.S. Voronov, private communication; see also E.D. Andrjukhina et al., Laser plasma containment in TOR-I Stellarator, Proc. Sixth European Conference on Controlled Fusion and Plasma Physics, Moscow, 1973, Vol. 1, pp.113 - 116

9. J.M. Dawson, On the production of plasma by giant pulse lasers, Phys. Fluids, Vol.7, No. 7, pp. 981-987 (1964)

10. Lyman Spitzer, Physics of Fully Ionized Gases, Intersci. Publ. Inc., N.Y. 1956

11. K. Büchl and T. Haering, Interferometric density measurements by a $CO_2$ laser in a laser produced plasma. Max-Planck-Institut für Plasmaphysik, Garching, Rept. No. 4/125 (1975)

12. Ya. B. Zeldovich and Yu. P. Raiser, Physics of Shock Waves and High-Temperature Hydrodynamic Phenomena, Academic Press, N.Y. and London, 1966

13. L.L. Lengyel, Numerical simulation of ionization instability with allowance for dissipative processes. Proc. 11th Symp. on Eng. Aspects of Magnetohydrodynamics, Cal. Inst. Techn., Pasadena, 1970, pp 193 - 198

14. A. Sommerfeld, Elektrodynamik, Bd. III, AK Verlagsgesellsch. Leipzig, 1964

15. W.R. Sears, Theoretical Aerodynamics, Lecture Notes, Grad School of Aeronaut. Eng., Cornell University, Ithacka, 1957

16. R.D. Richtmyer and K.W. Morton, Difference Methods for Initial Value Problems, Intersci. Publ. John Wiley & Sons, N.Y. 1967

17. A.A. Galeev and R.Z. Sagdeev, Parametric phenomena in a plasma,Nuclear Fusion, Vol. 13, pp. 603 - 621 (1973)

18. W.L. Kruer and J.M. Dawson, Anomalous high-frequency resistivity of plasma, Phys. Fluids, Vol. 15, No. 3, pp 446 - 453 (1972)